Activity of the *C. elegans* egg-laying behavior circuit is controlled by competing activation and feedback inhibition

Kevin M. Collins[1,2,6], Addys Bode[1], Robert W. Fernandez[2], Jessica E. Tanis[2,4], Jacob Brewer[2], Matthew S. Creamer[3,5], and Michael R. Koelle[2,3]

[1] Department of Biology, University of Miami, Coral Gables, FL USA

[2] Department of Molecular Biophysics and Biochemistry, Yale University, New Haven, CT USA

[3] Interdepartmental Neuroscience Program, Yale University, New Haven, CT USA

[4] Present address: Department of Biological Sciences, University of Delaware, Newark, DE USA

[5] Present address: Department of Molecular, Cellular, and Developmental Biology, Yale University, New Haven, CT USA

[6]To whom correspondence should be addressed:

kcollins@bio.miami.edu

Department of Biology

University of Miami

1301 Memorial Drive

Coral Gables, FL 33143

Tel: (305) 284-9058

Abstract

Like many behaviors, *Caenorhabditis elegans* egg laying alternates between inactive and active states. To understand how the underlying neural circuit turns the behavior on and off, we optically recorded circuit activity in behaving animals while manipulating circuit function using mutations, optogenetics, and drugs. In the active state, the circuit shows rhythmic activity phased with the body bends of locomotion. The serotonergic HSN command neurons initiate the active state, but accumulation of unlaid eggs also promotes the active state independent of the HSNs. The cholinergic VC motor neurons slow locomotion during egg-laying muscle contraction and egg release. The uv1 neuroendocrine cells mechanically sense passage of eggs through the vulva and release tyramine to inhibit egg laying, in part via the LGC-55 tyramine-gated Cl^- channel on the HSNs. Our results identify discrete signals that entrain or detach the circuit from the locomotion central pattern generator to produce active and inactive states.

35 **Introduction**

36 Neural circuits are the functional units underlying all thoughts and behaviors, but there is
37 as yet no neural circuit in any organism for which we know with precision how the many
38 signaling events among its cells together generate its activity. This would require, among other
39 things, understanding how neuromodulators shape activity at chemical and electrical synapses
40 to alter the excitability of specific cells in the circuit to generate regulated, dynamic patterns of
41 circuit responses and a coherent behavioral output. One approach to this problem is to analyze
42 small neural circuits typical of invertebrate model organisms, so that both the simplicity of the
43 circuits and the powerful experimental approaches uniquely possible within these systems can
44 provide a penetrating analysis (Marder, 2012).

45 *C. elegans* egg-laying behavior is controlled by a small circuit that offers many
46 experimental advantages for study (Schafer, 2006). This circuit, diagrammed in Figure 1A,
47 consists of two serotonergic Hermaphrodite Specific Neurons (HSNs) and six cholinergic
48 Ventral C neurons (VCs), each of which synapse onto a set of vulval muscles whose
49 contraction expels eggs. Four neuroendocrine uv1 cells also regulate egg laying (Jose et al.,
50 2007). Despite its anatomical simplicity, the egg-laying circuit produces a regulated, rhythmic
51 behavior that alternates between quiescent periods of about 20 minutes during which no egg
52 laying occurs, and active states lasting a few minutes during which ~5 eggs are laid
53 (Waggoner et al., 1998). Active states appear to result when the HSNs release serotonin that
54 signals through G protein coupled receptors on the vulval muscles to increase their excitability
55 (Waggoner et al., 1998; Shyn et al., 2003; Hapiak et al., 2009; Emtage et al., 2012). Strong
56 regulation by sensory stimuli is superimposed on the pattern of alternating behavioral states.
57 For example, carbon dioxide regulates neuropeptide release from head sensory neurons that

58 signal through receptors on the HSNs to inhibit egg laying (Ringstad and Horvitz, 2008; Hallem
59 et al., 2011). Worms also halt egg laying in the absence of food and restart the behavior when
60 re-fed (Daniels et al., 2000; Dong et al., 2000).

61 *C. elegans* egg laying has been studied for decades, and dozens of genes have been
62 identified by mutations that either reduce (Desai et al., 1988) or increase (Bany et al., 2003)
63 egg laying. Some of the identified genes encode ion channels that regulate cell and synaptic
64 electrical excitability (Elkes et al., 1997; Johnstone et al., 1997; Lee et al., 1997; Weinshenker
65 et al., 1999; Jospin et al., 2002; Jose et al., 2007; Collins and Koelle, 2013). Other identified
66 genes encode components of G protein signaling pathways that act in specific cells of the
67 circuit (Brundage et al., 1996; Koelle and Horvitz, 1996; Hajdu-Cronin et al., 1999; Miller et al.,
68 1999; Williams et al., 2007; Porter et al., 2010). These results suggest neuromodulators,
69 including serotonin, signal through G proteins to regulate the excitability of specific cells in the
70 circuit to control circuit activity and egg laying.

71 The ability to leverage egg-laying mutants to understand the molecular mechanisms that
72 initiate, sustain, and terminate the active state of egg laying has been limited by the tools
73 available to analyze activity in the cells of the egg-laying circuit. Ca^{2+} activity in cells in the
74 circuit was initially optically recorded in immobilized animals, which have limited ability to
75 engage in egg-laying behavior (Shyn et al., 2003; Zhang et al., 2008). More recently we
76 developed methods to optically record Ca^{2+} activity of the vulval muscles in moving animals as
77 they engage in normal egg-laying behavior. Using ratiometric imaging to correct for movement
78 and focus artifacts, and recording at 20 frames/sec for periods of up to one hour, we were able
79 to measure activity of the vulval muscles as animals cycled through active and inactive states
80 (Collins and Koelle, 2013; Li et al., 2013). Our recordings showed that the vulval muscles are

excited rhythmically in phase with the body bends of animal locomotion, and we proposed this was due to signaling from the cholinergic motor neurons, including the VCs, that are rhythmically active during locomotion. We found that a conserved ERG K^+ channel depresses response of the vulval muscles to excitation, thus maintaining the inactive behavior state, and we proposed that serotonin signaling onto vulval muscle receptors enhances vulval muscle excitability to allow the strong muscle contractions and egg release seen in the active state. We have now generated tools to carry out Ca^{2+} recordings in moving animals for each neuron type in the egg-laying circuit. Combining these recordings with precise manipulations of the circuit using mutations, optogenetics, and drugs allows us to deduce how specific signals from these cells drive specific features of circuit activity and behavior.

Results

Distinct patterns of activity in the egg-laying circuit accompany the active and inactive behavior states

We carried out long-term Ca^{2+} recordings of HSN and VC neuron activity in behaving animals using methods we developed previously for the vulval muscles (Collins and Koelle, 2013). We generated transgenic strains of *C. elegans* co-expressing the fluorescent Ca^{2+} reporter GCaMP5 and the Ca^{2+}-independent fluorescent protein mCherry specifically in the HSN or VC neurons, and used ratiometric imaging to record cell activity and egg-laying behavior as animals moved through active and inactive egg-laying states (Figure 1). Because of the large size of the egg-laying synapse, we were able to clearly observe Ca^{2+} transients localized to the presynaptic terminus in HSN (Figure 1B; Movie 1) and VC (Figure 1C; Movie 2).

103 For comparison, we also carried out Ca^{2+} recordings of vulval muscles, and as in our earlier
104 studies of these muscles, were able to clearly distinguish the weak twitching contractions
105 (Figure 1D; Movie 3) from the strong contractions that drove egg release (Figure 1E).

106 Through long-term Ca^{2+} imaging, we observed a striking increase in rhythmic activity in
107 the cells of the circuit that began prior to the first egg-laying event and persisted beyond the
108 last egg-laying event of each active state (Figure 1F). We defined the active state as one
109 minute before the first egg-laying event and one minute after the last egg-laying event.

110 We found that HSNs displayed long (~4 seconds at half-maximum amplitude) Ca^{2+}
111 transients that were largely consistent in waveform and amplitude, but that varied in occurring
112 either as single events or trains (Figure 1F). There was also significant HSN activity outside of
113 the active state, but HSN transients were more frequent during the active state (Figure 1G).
114 Active state HSN transients typically occurred in bursts, within which HSN transients occurred
115 every ~20 seconds (Figure 1G). Only 11% of HSN transients were accompanied by an egg
116 release (Figure 1H), but almost every egg-laying event occurred during an HSN transient
117 (Figure 1F; out of 49 total egg-laying events observed, 48 occurred within an HSN transient).

118 VC transients were shorter than HSN transients (~2 seconds at half-max) and variable
119 in amplitude. We rarely observed VC transients during the inactive state, but we found a clear
120 induction of transients during the active state (Movie 2; Figure 1F, G), and these transients
121 occurred in bursts around egg-laying events with an inter-transient interval of ~10 seconds,
122 about twice as frequent as seen for the HSNs. Although Ca^{2+} transients were most intense in
123 the VC presynaptic varicosities and axonal processes, they were also visible in all six VC cell
124 bodies, especially those of the VC4 and VC5 neurons that most closely flank the vulva (Figure
125 1C and Movie 2). Vulval muscle twitching and egg-laying contractions caused significant

126 mechanical deformation of the VC neurons. 34% of VC transients were accompanied by an
127 egg release, a larger fraction than seen for HSN and vulval muscle Ca^{2+} transients (Figure 3H,
128 p <0.0001; Fisher's exact test). Every egg-release event was accompanied by a VC transient.
129 There was no correlation seen between the magnitudes of VC or HSN transients that did or did
130 not coincide with egg release, while the magnitude of muscle Ca^{2+} transients that resulted in
131 egg laying were ~4-fold larger than the muscle twitch transients that did not release eggs
132 (Figure 1H).

133 The close apposition of HSN, VC, and vulval muscle synaptic regions prevented us from
134 simultaneously imaging more than one cell type, but we were able to compare timing of activity
135 in the different cells using the moment of egg release as an objective landmark. HSN Ca^{2+}
136 transients peaked ~2 seconds prior to egg release (Figure 1I) and decayed slowly. Shorter VC
137 Ca^{2+} transients followed HSN activity, peaking ~0.1 seconds before egg release. Vulval muscle
138 Ca^{2+} transients peaked with egg laying. We also tracked vulval muscle contraction by
139 measuring the size and fluorescence intensity of the mCherry labeled muscles, and saw that
140 muscle relaxation and decay of vulval muscle Ca^{2+} immediately followed egg release (Figure
141 1I).

142

143 **HSN, VC, and vulval muscle activity are rhythmic and phased with animal locomotion**

144 Previous work showed that timing of egg-laying events was not rhythmic but followed a
145 Poisson distribution (Waggoner et al., 1998). However, we found that HSN, VC, and vulval
146 muscles showed rhythmic activity during the egg-laying active state. We calculated the power
147 spectra of HSN, VC, and vulval muscle Ca^{2+} traces, and we observed three activity rhythms in

148 the egg-laying circuit during the active state (Figures 2A-E). Rhythms in HSN and VC were
149 similar, peaking at ~50 mHz with smaller peaks observed at ~100 and ~140 mHz (Figures 2B,
150 2C). The 50 mHz rhythm was also clearly evident in the vulval muscles (Figure 2D), but the
151 100 mHz peak was significantly stronger (Figure 2E). These results show that despite egg-
152 laying behavior being aperiodic, circuit activity underlying that behavior is rhythmic.

153 What is the source of circuit rhythmicity? *C. elegans* moves with sinusoidal body bends
154 consisting of rhythmic_waves of body-wall muscle contraction driven by the Ventral A and B
155 (VA/VB) ventral nerve cord motor neurons. We previously observed that vulval muscle Ca^{2+}
156 transients tend to occur when the vulva is at a particular phase of the locomotion body bend
157 (Collins and Koelle, 2013), suggesting rhythmic activity in the locomotor circuit may be the
158 source of rhythmicity in the egg-laying circuit. Using our video recordings of Ca^{2+} activity in
159 moving animals, we examined whether HSN and VC activity, like vulval muscle activity, are
160 phased with locomotion. Thus we determined timing of the peaks of HSN, VC, and vulval
161 muscle Ca^{2+} transients relative to when the vulva passed through the previous and subsequent
162 most contracted or relaxed state of a body bend (Figure 2–figure supplement 1, see Materials
163 and Methods). The results were plotted on histograms with ventral contraction at 0 and 360°,
164 ventral relaxation at 180°, and intermediate phases of body bends at the angles in between
165 (Figure 2F-I). We found that the HSN, VC, and vulval muscle Ca^{2+} transients occurred when
166 the vulva was at particular phases of the locomotor body bend. HSN transients just prior to egg
167 release reached their maximum at ~180°, when the vulva and adjacent body wall muscles
168 were at their most relaxed state (Figure 2G). VC and vulval muscle transients that
169 accompanied egg laying occurred later, starting at ~225° (Figure 2H and 2I). HSN transients
170 that did not result in egg laying showed no clear evidence of phasing (Figure 2G). In contrast,

171 VC transients and vulval muscle twitch transients that did not lead to egg release were still
172 phased, but delayed by ~45° toward the most ventral contracted state. These results confirm
173 our previous observations that vulval muscle twitching and egg-laying activity are phased with
174 locomotion (Collins and Koelle, 2013). These results extend that analysis to show that HSN,
175 VC, and vulval muscle activity during egg laying events are rhythmic, phased with locomotion,
176 and occur earlier in the body bend cycle, when the adjacent body wall muscles are in a more
177 relaxed state.

178

179 **Optogenetic activation of HSNs initiates the egg-laying active state**

180 To directly test how neurotransmitter signaling from the HSNs regulates egg-laying
181 circuit activity, we used the *egl-6* promoter to express Channelrhodopsin-2 in the HSNs
182 (Emtage et al., 2012), allowing us to drive neurotransmitter release specifically from the HSNs
183 with blue light. We repeated the observation of Emtage et al. (2012) that optogenetic activation
184 of HSNs stimulates egg-laying behavior (Movie 4), but we activated the HSNs while
185 simultaneously recording behavior and Ca^{2+} activity in the VCs (Figure 3A) or vulval muscles
186 (Figure 3B). We found that activation of HSNs resulted in circuit activity reminiscent of a
187 spontaneous active state, including rhythmic Ca^{2+} activity of both VCs and vulval muscles, and
188 egg-laying events that accompanied a subset of these Ca^{2+} transients. Some differences from
189 a spontaneous active state were notable. Almost every VC transient after optogenetic HSN
190 activation was accompanied by an egg-laying event, whereas only one third of VC transients
191 during spontaneous active states were accompanied by egg-laying events. These results
192 suggest that the high level of HSN activity after optogenetic activation induces strong coupling
193 of VC and vulval muscle excitation.

194 During both spontaneous and optogenetically-induced active states, rhythmic vulval
195 muscle twitches occur far more frequently than do VC transients, suggesting these twitches
196 are excited by something other than the VCs. Careful observation shows that the most
197 dramatic Ca^{2+} changes during vulval muscle twitching occur at the ventral tips of the vm1
198 muscles (Figure 1D). The VCs innervate vm2 muscles but not the vm1 muscles. The vm1
199 muscles are instead innervated by the VB6 and VA7 neurons that also release acetylcholine to
200 drive body wall muscle contraction for locomotion (White, J.G. et al., 1986). Consistent with
201 this, vm1 twitching occurs at the same time the adjacent ventral body wall muscles are
202 contracting during locomotion (Figure 2D). Increased electrical excitability of the vulval muscles
203 during a spontaneous or optogenetically-induced active state may allow for vm1 excitation by
204 VB6/VA7 with each body bend.

205

206 **VC neuron activity helps coordinate egg laying and locomotion**

207 Our observation that VC activity always accompanies egg release (Figure 1I and 3A) is
208 consistent with a proposal that the VCs release acetylcholine that signals through vulval
209 muscle nicotinic receptors to drive egg laying (Waggoner et al., 2000; Kim et al., 2001). While
210 VC4 and VC5 make extensive synapses onto the vm2 muscles, VC1-3 and VC6 make
211 extensive, distributed synapses onto the ventral body wall muscles (White et al., 1976). How
212 VC activity during egg laying might affect body wall muscle contraction has not been examined.
213 We optogenetically activated the HSNs to induce active states and recorded animal speed
214 around egg-laying events (Figure 3C). We found a clear and significant reduction of locomotion
215 speed beginning ~1 s before egg release, a time when VC activity is increasing (Figure 1I).
216 Locomotion speed recovered immediately after egg release (Figure 3C). These results are

217 consistent with the hypothesis that acetylcholine released from the VCs slows locomotion
218 during egg laying.

219 To test directly how VC activity regulates locomotion and egg laying, we used a *lin-11*
220 promoter fragment to express Channelrhodopsin-2 specifically in the VCs (Bany et al., 2003).
221 Optogenetic activation of the VCs was not sufficient to drive egg laying (Figure 3F), but did
222 lead to a rapid shortening of the body (Movie 5 and Figure 3D) and cessation of locomotion
223 (Figure 3E). The shortening phenotype seen in VC ChR2 animals after blue light exposure
224 closely resembles that seen for optogenetic activation of the body wall muscles (Nagel et al.,
225 2005), except the head and tail of VC-activated animals were still mobile and active, consistent
226 with the fact that VC neurons innervate only the central body wall muscles (White et al., 1976).
227 Our results indicate that while VC activity immediately precedes egg-laying events, it is not
228 sufficient to drive egg release. Optogenetic VC activation is sufficient to produce a slowing of
229 locomotion as seen during egg-laying events. In contrast, HSN activity is sufficient to induce all
230 of the hallmarks of the active state, including rhythmic vulval muscle twitching, VC transients,
231 and the coordinated vulval muscle contractions that produce egg-laying events.

232

233 **Animals lacking HSNs still enter the egg-laying active state**

234 We next tested whether HSN activity was necessary for circuit activity by recording
235 vulval muscle activity in *egl-1(dm)* mutants, which lack HSN neurons (Trent et al., 1983).
236 Animals lacking HSNs have a substantial lengthening of the inactive state (Waggoner et al.,
237 1998) and are strongly egg-laying defective, accumulating ~50 eggs in the uterus rather than
238 the 12-15 seen in the wild type (Trent et al., 1983). We expected to find that loss of HSNs led

239 to a dramatic reduction in vulval muscle activity. Surprisingly, we found the opposite; animals
240 lacking HSNs had more frequent vulval muscle Ca^{2+} transients during the inactive state and
241 robust activity during infrequent active states that led to multiple eggs being laid in a short
242 period (compare Figures 4A and 4B; quantitation in Figure 4C). There was a significant
243 reduction in the amplitude of vulval muscle Ca^{2+} transients during egg laying in *egl-1(dm)*
244 mutants while the amplitude of twitch Ca^{2+} transients was unaffected (Fig. 4D). Vulval muscle
245 activity in *egl-1(dm)* mutants lacking HSNs resembled the frequent yet uncoordinated vulval
246 muscle activity found in animals missing the vm2 vulval muscle arms onto which the HSNs
247 normally make synapses (Li et al., 2013). Such activity involves asynchronous contraction of
248 the anterior and posterior vulval muscles, which is ineffective at allowing egg release. One
249 quantitative measure of this asynchrony is that overall vulval muscle Ca^{2+} transient peaks in
250 *egl-1(dm)* mutants were longer in duration, likely resulting in individual muscle cells beginning
251 their transients at different times (Figure 4E). Vulval muscle Ca^{2+} transients in animals lacking
252 HSNs remained phased with locomotion, including the ~45° advance in phase of vulval muscle
253 activity that results in egg-laying events (Figure 4–figure supplement 1). These results suggest
254 that the HSNs are necessary to coordinate contraction of anterior and posterior vulval muscles,
255 and that signals from other cells besides the HSNs can also induce the egg-laying active state.

256 We hypothesized that accumulating unlaid eggs could stretch the uterus or body,
257 leading to signals responsible for the increased activity of the vulval muscles independent of
258 neurotransmitter signaling from the HSNs. To test if egg accumulation contributed to the onset
259 of the active phase, we sterilized animals with FUDR (Mitchell et al., 1979), a DNA synthesis
260 inhibitor that blocks germ line cell division and thus egg production. FUDR-treated animals had
261 a dramatic reduction of vulval muscle activity and appeared to be stuck in the inactive state,

262 with no egg-laying transients observed (Figures 4A and 4B). The inhibition of vulval muscle
263 activity by FUDR occurred in both wild-type animals and HSN-deficient *egl-1(dm)* mutants
264 (Figures 4C and 4D). The residual vulval muscle Ca^{2+} twitch transients in FUDR-treated
265 animals had phasing identical to those seen in the inactive state of untreated animals (Figure
266 4–figure supplement 1). These results suggest that germ line activity and/or the accumulation
267 of eggs in the uterus is required to initiate the egg-laying active state.

268

269 **The uv1 neuroendocrine cells are mechanically deformed and activated by egg-laying**
270 **events**

271 We previously identified a role for the uv1 neuroendocrine cells in inhibiting egg-laying
272 behavior (Jose et al., 2007). The four uv1 cells sit at the junction between the uterine lumen
273 and the vulval canal (Newman and Sternberg, 1996), and as such are positioned to
274 mechanically sense the accumulation of unlaid eggs in the uterus and/or passage of eggs
275 through the vulval canal as they are laid. To record uv1 Ca^{2+} activity, we co-expressed
276 GCaMP5 and mCherry in uv1 from the *ocr-2* promoter and made recordings in behaving
277 animals. We found that the uv1 cells were mechanically deformed as each egg passed through
278 the vulva, and then showed strong Ca^{2+} transients after egg release (Figure 5A-B; Movie 5).
279 Egg-laying events did not always trigger Ca^{2+} transients in uv1, with uv1-silent events usually
280 being the first or last within an active state (data not shown). We also observed weaker uv1
281 Ca^{2+} transients a few minutes before or after the egg-laying active state (Figure 5B-D).
282 Because these were not closely associated with egg-laying events their functional importance
283 remains unclear. Typical active state uv1 Ca^{2+} transients began immediately with or slightly
284 before egg release, coinciding with the initial mechanical deformation of uv1 caused by the egg,

285 with the Ca^{2+} transient peak occurring ~2 seconds later (Figure 5E). Based on the position of
286 the uv1 cells, their morphological deformations during passage of eggs, and the timing of uv1
287 Ca^{2+} transients, our data suggest the uv1 cells are mechanically activated by eggs passing
288 through the vulva during egg laying.

289

290 **Tyramine signals through LGC-55 receptors to inhibit HSN activity and egg laying**

291 The uv1 cells make the biogenic amine neurotransmitter tyramine, and *tdc-1* mutations
292 that disrupt tyramine biosynthesis lead to increased egg-laying behaviors (Alkema et al., 2005).
293 We found that exogenous tyramine reduced egg laying in wild-type animals (Figure 6A). To
294 identify targets of tyramine inhibition, we tested response to exogenous tyramine in strains
295 mutant for three known *C. elegans* tyramine receptors. Animals lacking *lgc-55*, which encodes
296 a tyramine-gated Cl^- channel, showed resistance to inhibition by exogenous tyramine (Figure
297 6A), although tyramine at high levels still had a residual ability to reduce egg laying in *lgc-55*
298 mutants (Figure 6B). We transformed into *C. elegans* a fosmid transgene containing the full-
299 length *lgc-55* gene fused to GFP coding sequences, and found LGC-55 is expressed in the
300 HSNs, uv1, and vulval muscles (Figure 6C and Pirri et al., 2009). Re-expression of LGC-55
301 specifically in HSN from the *tph-1* promoter restored tyramine sensitivity to *lgc-55* mutants
302 (Figure 6D). We have previously shown that two Cl^- extruding transporters, KCC-2 and ABTS-1,
303 are expressed in the HSNs where they promote the development of inhibitory ligand-gated Cl^-
304 channel signaling (Tanis et al., 2009; Bellemer et al., 2011). These data suggest that tyramine
305 signaling through LGC-55 would hyperpolarize the HSN and inhibit activity. To test this directly,
306 we compared HSN activity in wild-type and *lgc-55* mutant animals. We observed a significant
307 increase in the frequency of Ca^{2+} transients in HSNs of *lgc-55* mutant animals (Figures 6E and

308 6F) in both the inactive and active states of egg-laying behavior. Mean HSN inter-transient
309 intervals in wild-type animals were 41±5 seconds in the inactive state and 17±2 seconds during
310 the active state, while intervals in *lgc-55* mutants were reduced to 22±2 seconds in the inactive
311 state and 13±1 seconds during the active state. Thus, the absence of inhibitory feedback by
312 tyramine signaling onto the HSNs leads to increased activity in both the active and inactive
313 egg-laying behavior states.

314

315 **Discussion**

316 Using a combination of optogenetic, molecular genetic, and Ca^{2+} imaging approaches,
317 we show an unexpected level of coordination of *C. elegans* egg-laying circuit activity by the
318 rhythm of locomotion and by egg production. Using recordings of cell activity in behaving
319 animals as they transition from the inactive to active egg-laying states, we were able to show
320 that circuit activity is diminished during the inactive state, strongly increased and rhythmic
321 during the active state, and this rhythm is phased with sinusoidal locomotion. Sterilization
322 eliminated the active state rhythm, locking animals in the inactive state. Our results suggest
323 that activity in the egg-laying circuit, like that of many other modulated motor circuits, responds
324 to rhythmic input from central pattern generators (Marder et al., 2015).

325 A working model shown in Figure 7 explains how different inputs into the egg-laying
326 circuit are responsible for the inactive state and the active state rhythms observed during egg-
327 laying behavior. Active state vulval muscle Ca^{2+} transients peak rhythmically each time the
328 vulva approaches a ventral body bend, the point at which the cholinergic VB and VA motor
329 neurons release acetylcholine to rhythmically excite both the vm1 muscles and adjacent

330 ventral body wall muscles during locomotion. During the inactive state, K^+ channels including
331 ERG depress vulval muscle excitability below threshold, explaining why we fail to observe
332 vulval muscle activity with each body bend during this state (Collins and Koelle, 2013). While
333 we observe rhythmic activity in the HSNs in the active phase, the periodicity and phasing of
334 HSN activity does not correlate with that of locomotion. Consistent with this, previous work
335 found changes in osmolarity can drive rhythmic HSN activity even in immobilized animals
336 (Zhang et al., 2008). Thus HSN rhythmic activity is independent of locomotion, although we
337 found HSN Ca^{2+} transients that happen to fall at a specific phase of locomotor body bends are
338 more likely to be followed by egg release. We propose that release of serotonin from the HSNs,
339 along with an unknown signal resulting from mechanical stretch of the uterus by accumulating
340 eggs, together raise vulval muscle electrical excitability to result in the active state during which
341 the vulval muscles undergo rhythmic twitching or egg laying contractions in response to the
342 same cholinergic VA and VB neurons that drive locomotor body bends. This model accounts
343 for the phasing of vm1 transients with body bends, although egg-laying events require
344 additional activity in the vm2 muscles that results in the coordinated contraction of all vm
345 muscles that results in egg release. We found that vm transients that lead to egg release are
346 on average slightly phase advanced relative to those that do not. This phase advance could
347 from the excitatory input onto the vm2 muscles occurring earlier in the body bend, and
348 candidates for this input are the HSNs and VCs, both of which synapse onto the vm2 muscles
349 and have phased activity during egg-laying events. The functional purpose of this phase
350 advance may be mechanical. Passage of each 25x40μm egg requires contraction of vm1 and
351 vm2 muscles on both the anterior and posterior sides of the vulva (Li et al., 2013). There may
352 not be sufficient room for vulva to fully open and release egg unless the adjacent body wall
353 muscles are in a contracted state.

354 The HSNs are command neurons that integrate diverse sensory inputs and initiate the
355 ~2 minute active state of the egg-laying circuit. Optogenetic activation of HSNs recapitulates
356 features of the active state including phased VC and vulval muscle activity and multiple egg-
357 laying events. However, stimulation of the HSNs fails to drive tetanic contraction of the vulval
358 muscles as would be predicted for a motor neuron releasing a fast-acting neurotransmitter.
359 Instead, HSN makes and releases the neuromodulator serotonin which signals through G
360 protein coupled serotonin receptors to activate the vulval muscles (Desai et al., 1988; Shyn et
361 al., 2003; Carnell et al., 2005; Hobson et al., 2006; Hapiak et al., 2009). The HSNs also
362 release serotonin onto the AVF interneurons in the nerve ring to promote a state of locomotion
363 arousal that accompanies the active state (Hardaker et al., 2001). Animals defective in
364 serotonin signaling have reduced egg laying (Tanis et al., 2008), but this defect is not as
365 severe as that of *egl-1(dm)* animals missing HSNs (Trent et al., 1983), suggesting HSN
366 releases additional neurotransmitters. We found that optogenetic activation of HSNs leads to
367 rhythmic activity of VC neurons, which are not known to express serotonin receptors, so an
368 unknown signal derived from HSN could directly activate VCs, as depicted in the Figure 7
369 model.

370 How is HSN activity controlled? The HSNs receive little synaptic input near the vulval
371 except from the PLM mechanosensory neurons (White, J.G. et al., 1986). The PLMs inhibit
372 HSN activity and egg laying in response to gentle touch (Zhang et al., 2008), but recent work
373 indicates the PLM neurons are also deformed during normal patterns of locomotion that could
374 contribute to rhythmic activity seen in HSN during egg laying (Topalidou et al., 2012).
375 Neuroendocrine signaling also regulates HSN activity. *flp-10* and *flp-17* neuropeptides are
376 released from the CO_2-responsive BAG neurons in the head, and these neuropeptides signal

377 through EGL-6 receptor and $G\alpha_o$ to activate IRK channels that inhibit HSN activity and egg
378 laying (Ringstad and Horvitz, 2008; Hallem et al., 2011; Emtage et al., 2012). Because loss of
379 EGL-6 or IRK channels do not increase egg laying as much as cell-specific inhibition of $G\alpha_o$,
380 there must be additional receptors and effectors of $G\alpha_o$ that inhibit HSN activity. $G\alpha_q$ signaling
381 opposes $G\alpha_o$ to increase serotonin release from the HSNs (Tanis et al., 2008), but the ligands
382 and receptors that activate $G\alpha_q$ have not yet been identified. Because we find that HSN Ca^{2+}
383 transients vary more in frequency than amplitude, we propose that these diverse sensory
384 signals increase or reduce the probability that HSN reaches a threshold potential that can
385 initiate, sustain, or terminate HSN activity and thus the active behavior state of the egg-laying
386 circuit.

387 We have also identified an HSN-independent mechanism that induces the active state.
388 Mutants lacking HSNs are strongly egg-laying defective, but eventually enter active states with
389 properly phased vulval muscle twitching and egg-laying transients. The active state was
390 eliminated in animals sterilized by FUDR, reducing vulval muscle activity and phasing to that
391 seen in the inactive state. Recent work has identified the gonad as an important site of
392 regulation for adult-specific behaviors in *C. elegans* (Fujiwara et al., 2016). We propose that
393 the accumulation of unlaid eggs in the uterus, perhaps leading to mechanical stretch, provides
394 an essential, permissive signal for entry into the active state. Several steps during embryo
395 production and maturation could regulate entry into the active state to result in the ~20 period
396 of the egg-laying inactive state. Animals grown on food generate one new oocyte from each of
397 two gonad arms every ~10 minutes, balancing out the 3-5 eggs laid in the ~2 minute active
398 state that occurs every ~20 minutes, to result in a ~constant number of unlaid eggs in the
399 uterus (McCarter et al., 1999). New embryos are moved by gonadal sheath contractions into

400 the spermatheca for fertilization and deposition into the uterus. Excitable cells drive each of
401 these steps, providing potential sources of regulation by cell signaling and sensory feedback
402 (Kariya et al., 2004). Eight uterine muscles line the uterine lumen and form gap junctions with
403 the vm2 muscles (White, J.G. et al., 1986), and the addition of unlaid eggs into the uterus
404 could induce a mechanical stretch that cross-excites the vm2 muscles. Future work will be
405 required to understand how the accumulation of unlaid eggs promotes the active state.

406 Our results strongly imply that acetylcholine released from the VC motor neurons slows
407 locomotion during vulval muscle contraction. We found that animal locomotion slows during
408 egg release, and that optogenetic activation of the VC neurons halts movement and results in
409 body wall muscle contraction and animal shortening. This function of the VCs is likely via
410 acetylcholine signaling through nicotinic receptors expressed on ventral body wall muscles and
411 neurons that regulate locomotion (White, J.G. et al., 1986; Nagel et al., 2005). The effect of VC
412 activity to slow locomotion and contract body wall muscles may help compress the body and
413 uterus to encourage expulsion of eggs, analogous to the role of body wall muscle contraction in
414 facilitating defecation (Liu and Thomas, 1994).

415 Our results provide more complex evidence as to whether VC acetylcholine also directly
416 triggers egg release. We found that VC activity always accompanies egg-laying contractions of
417 the vulval muscles. The vulval muscles also express nicotinic acetylcholine receptors, and
418 receptor agonists including levamisole and nicotine stimulate egg laying (Weinshenker et al.,
419 1995; Waggoner et al., 2000). However, we found little correlation between the strength of the
420 VC activity and whether an egg is laid (Figure 1H), and that optogenetic activation of the VC
421 neurons fails to drive egg laying. Further, VC-defective and acetylcholine-deficient mutants
422 have *increased* egg-laying behavior (Bany et al., 2003; Ringstad and Horvitz, 2008). These

423 data together are consistent with a model in which acetylcholine released from the VA/VB
424 motor neurons signal through nicotinic receptors on the vm1 muscles to stimulate rhythmic
425 vulval muscle twitching, which combined with acetylcholine released from the VC neurons to
426 similarly excite the vm2 muscles results in egg laying. High levels of VC activity, such as
427 occurs during optogenetic activation, may drive release of additional signals, such as
428 neuropeptides, that inhibit egg-laying circuit activity (Bany et al., 2003; Banerjee et al., 2016),
429 or by freezing locomotion may feedback to halt the VA/VB activity required to drive vm1
430 contraction.

431 How is VC activity controlled? The VC neurons are unusual in that they are largely
432 presynaptic, only receiving input from each other and the HSNs. As noted above, optogenetic
433 activation of HSNs results in VC activity, suggesting a currently unknown signal from HSN
434 directly activates VCs. A second possible input onto VCs is suggested by the fact that the VC
435 neurons extend processes devoid of synapses dorsally along the vulval hypodermis that could
436 be mechanosensory (White, J.G. et al., 1986). Thus, rhythmic VC activity could be stimulated
437 mechanically by body bends or by a humoral signal released from the locomotor circuit (Hu et
438 al., 2011). Further, VC activity could be mechanically stimulated by vulval muscle contraction
439 (Zhang et al., 2010), particularly as we observed mechanical deformation of VC presynaptic
440 termini during strong twitching and egg-laying contractions. In this way, the VCs could act like
441 baroreceptors–mechanically activated by vulval muscle contraction to drive contraction of the
442 body wall muscles that results in animal slowing until the feedback of egg release. In this
443 model, the coordination of locomotion and egg laying by tying both behaviors to the same
444 central pattern generator allows productive egg release.

445 The uv1 neuroendocrine cells inform the circuit that eggs have been successfully laid.
446 Passage of eggs through the vulva mechanically deforms the uv1 cells and triggers a strong
447 Ca^{2+} transient. Our results suggest this activates uv1 to release tyramine that inhibits egg-
448 laying, at least in part via the LGC-55 receptor on the HSN neurons. Active states last ~2
449 minutes, and inhibitory tyramine release from uv1 could provide a feedback signal that
450 terminates activity in the circuit. The four uv1 cells have a unique structural position in the
451 vulva that may explain how they become activated during egg laying (Newman et al., 1996).
452 uv1 cells extend processes that contact and make adherens junctions with the ventral vulF
453 vulval cells. uv1 cells also makes dorsal attachments to utse, a large, H-shaped multinucleate
454 uterine seam cell that attaches the uterus to the lateral epidermis and that functions as a
455 hymen broken by the first egg-laying event. The acute mechanical strain on vulF, uv1, and/or
456 utse during egg passage could mechanically activate ion channels. Previous work has shown
457 uv1 expresses several TRPV channels that may be mechanosensory and contribute to this
458 response (Jose et al., 2007). A dominant-negative OCR-2 mutant expressed in uv1 leads to
459 hyperactive egg-laying behavior phenotype. We still observe Ca^{2+} transients in uv1 after egg-
460 laying events in this *ocr-2(vs29)* mutant (data not shown), suggesting other channels contribute
461 to the uv1 activity we see after egg laying. Although our results indicate that uv1 releases
462 tyramine to inhibit the HSNs via LGC-55, this signaling event does not fully explain the ability of
463 uv1 cells to inhibit the egg-laying circuit. We found that inhibition of egg laying by exogenous
464 tyramine is reduced but not eliminated in *lgc-55* null mutants, suggesting other tyramine
465 receptors help terminate the active state. The uv1 cells also make *nlp-7* and *flp-11*, two
466 neuropeptides that inhibit HSN activity and egg-laying behavior (Banerjee et al., submitted),
467 and the identification of the receptors and signaling pathways through which they inhibit

468 serotonin release will help to more fully understand how activity of the egg-laying circuit is
469 terminated.

470 Every neural circuit may require specific signals to initiate activity when its function is
471 required, signals to coordinate the dynamic activity of its various cells, and mechanisms to
472 determine when the circuit has successfully completed its task and signal to turn off activity.
473 Many circuits also must respond to specific signals from central pattern generators that
474 coordinate the activity of multiple circuits. A great challenge is to reduce these abstract
475 concepts to concrete, specific mechanisms in the case of a real circuit. For the *C. elegans* egg-
476 laying circuit, signals in each of the categories outlined above are now identified, albeit in
477 varying levels of detail and completeness. Continuing analysis of the *C. elegans* egg-laying
478 circuit using recordings of Ca^{2+} activity in behaving animals, combined with genetic,
479 optogenetic, and pharmacological manipulation, provides a path towards detailed
480 understanding the mechanisms that control activity of this model circuit.

481

482 **Materials and Methods**

483 Nematode Culture, Strains, and Maintenance

484 *Caenorhabditis elegans* strains were maintained as hermaphrodites at 20°C on Nematode
485 Growth Medium (NGM) agar plates with *E. coli* OP50 as a source of food as described
486 (Brenner, 1974). All strains are derived from the Bristol N2 wild-type strain, and all assays
487 were performed using age-matched adult hermaphrodites ~24 hours past the late L4 stage
488 using recommended sample sizes (Chase and Koelle, 2004). Animals were treated with 0.1
489 mg/ml floxuridine (FUDR) at a late L4 stage when all non-germline cell divisions are complete.
490 A list of strains, mutants, and transgenes used in this study can be found in Table 1.

491

492 Molecular Biology and Transgenes

493 *Vulval muscles:* GCaMP5G (Akerboom et al., 2012) and mCherry were expressed in the
494 vulval muscles from the *unc-103e* promoter as previously described (Collins and Koelle, 2013).
495 Briefly, pKMC274 (GCaMP5, 20ng/*µ*l) and pKMC257 (mCherry, 2ng/*µ*l) were co-injected along
496 with the pL15EK *lin-15* rescue plasmid (50ng/*µ*l) into LX1832 *lite-1(ce314), lin-15(n765ts)* X
497 animals. The GCaMP5/mCherry extrachromosomal transgene produced was chromosomally
498 integrated using UV/TMP mutagenesis, creating the integrated transgene *vsIs164*, and the
499 resulting transgenic animals were backcrossed to the LX1832 parental line six times.

500 *HSN:* GCaMP5G and mCherry were expressed in the HSN motor neurons using the *nlp-3*
501 promoter. mCherry and GCaMP5G coding sequences were ligated into pJB9 bearing the *nlp-3*
502 promoter and *nlp-3* 3' untranslated region, and the resulting plasmids (GCaMP5, pKMC300,
503 80ng/*µ*l; mCherry, pKMC299, 20ng/*µ*l) were co-injected with pL15EK (50ng/*µ*l) into LX1832

504 worms. The extrachromosomal transgene produced was integrated with UV/TMP, creating the
505 integrated transgene *vsIs183,* and the resulting transgenic animals were backcrossed to the
506 LX1832 parental line six times. The *wzIs30* transgene expressing Channelrhodopsin-2 from
507 the *egl-6* promoter has been described (Emtage et al., 2012).

508 *VC:* GCaMP5G and mCherry were expressed in the VC motor neurons using pKMC145, a
509 pDM4-based plasmid bearing a *lin-11* enhancer region fused to the *pes-10* basal promoter with
510 a modified multiple cloning site (Bany et al., 2003; Tanis et al., 2008). Derivatives expressing
511 GCaMP5 (pKMC273, 80ng/*µ*l) and mCherry (pKMC275, 30ng/*µ*l) were co-injected with
512 pL15EK (50ng/*µ*l) into LX1832 worms. The extrachromosomal transgene produced was
513 integrated with UV/TMP, creating the transgene *vsIs172*, and transgenic animals were
514 backcrossed to the LX1832 parental line six times. To activate the VCs optogenetically, coding
515 sequences for ChR2-YFP bearing the H134R, T159C mutations (Erbguth et al., 2012) were
516 amplified by PCR, ligated into pKMC145 to generate pKMC283, injected at 80ng/*µ*l into
517 LX1832 along with pL15EK at 50ng/*µ*l. The extrachromosomal transgene produced was
518 integrated with UV/TMP creating the transgene *keyIs3,* and the resulting animals were
519 backcrossed to LX1832 parental line six times.

520 *uv1:* GCaMP5G and mCherry were expressed in uv1 using the *ocr-2* promoter. GCaMP5 and
521 mCherry coding sequences were ligated into pJT79 between the *ocr-2* promoter and 3'
522 untranslated region (Jose et al., 2007) to generate plasmids pKMC281 and pKMC284,
523 respectively. Long-range PCR products amplified from these plasmids were injected into
524 worms at 80ng/*µ*l each along with pL15EK (50ng/*µ*l) as previously described (Jose et al., 2007).
525 The extrachromosomal transgene produced was integrated with UV/TMP creating the

526 transgene *vsIs177*, and the resulting animals were backcrossed to the LX1832 parental line six
527 times.

528 *lgc-55*: A ~40 kb genomic fosmid clone (WRM063D_A12) recombineered to express LGC-55
529 tagged with GFP at the C-terminus (Sarov et al., 2012) was injected at 100ng/μl into LX2081
530 *unc-119(ed3)* mutant animals expressing TagRFP pan-neuronally to generate the strain
531 LX2126. These animals were then crossed with LX2096 animals to exchange pan-neural
532 mCherry transgene for one that expresses in the vulval muscles, generating LX2126.
533 Fluorescence was visualized on immobilized animals with a 63x water objective on a Zeiss
534 LSM 710 Duo confocal microscope. For cell-specific rescue, LGC-55 was expressed in the
535 HSN neurons of *lgc-55* mutant animals using the *tph-1* promoter. Briefly, a *lgc-55* cDNA (Pirri
536 et al., 2009) was inserted into pJM66A plasmid (Moresco and Koelle, 2004) to generate
537 pJT105. pJT105, or a GFP-expressing control plasmid (pJM60A), was injected at 100ng/μl
538 along with pL15EK rescue plasmid (50ng/μl) into *lgc-55(tm2913); lin-15(n765ts)* double mutant
539 animals. Egg-laying behavior was analyzed in six independent transgenic lines expressing
540 LGC-55 or GFP, and one strain of each were kept for long-term storage.

541

542 Ratiometric Ca^{2+} Imaging

543 Animals were mounted between glass coverslips and chunked sections of NGM plates for
544 imaging as described (Collins and Koelle, 2013; Li et al., 2013). The stage and focus were
545 adjusted manually to keep the egg-laying system in view during recording periods. Long-term
546 recordings were cropped to 10-30 minutes with the first egg-laying event at 5 minutes. Three
547 different imaging systems were used to collect recordings, and each gave quantitatively similar

548 results. First, single, two-channel confocal slices (18 μm thick) of GCaMP5 and mCherry
549 fluorescence were collected through a 20x Plan Apochromat objective (0.8NA) using a Zeiss
550 Axio Observer microscope and recorded at 20 fps at 256x256 pixel resolution, 16-bit depth
551 using a 710 Duo LIVE scanner as described previously (Collins and Koelle, 2013; Li et al.,
552 2013). Second, widefield GCaMP5 and mCherry fluorescence was imaged through a 20x Plan
553 Apochromat objective (0.8NA) using a Zeiss Axio Observer microscope, and the GCaMP5 and
554 mCherry fluorescence was separated using a W-View Gemini image splitter at 20 fps at
555 256x256 pixel resolution, 16-bit depth onto a single, 4x4 binned Hamamatsu ORCA Flash 4.0
556 V2 sCMOS sensor after excitation with 470 nm and 590 nm LEDs (Zeiss Colibri.2). Third,
557 single, two-channel confocal slices (20 μm thick) of GCaMP5 and mCherry fluorescence were
558 collected using an inverted Leica TCS SP5 confocal microscope with the resonant scanner
559 running at 8,000Hz and collected at 20 fps at 256x256 pixel resolution, 12-bit depth after 2x
560 digital zoom.

561 Quantitative ratiometric analysis was performed after importing image sequences into
562 Volocity (Perkin Elmer). GCaMP5/mCherry ratios were calculated, and pixels with mCherry
563 fluorescence intensities ~2 standard deviations above background were selected as objects for
564 mean ratio measurement. While the Volocity algorithm set with these parameters typically
565 identified the vulval muscles and uv1 cells as a single object, the complex morphology of the
566 HSN and VC neurons often led to the cells being found as two or more objects within each
567 video frame. These were rejoined using a custom script in MATLAB (Mathworks). The ratio of
568 the joined object was scaled in proportion to the area of each component object to generate an
569 area-adjusted GCaMP5/mCherry ratio. The ratio data were then smoothed using a 150 msec
570 (three timepoint) rolling average, and the lowest 10% of the GCaMP5/mCherry ratio values

571 over the entire recording period were averaged to establish a ΔR/R baseline. Ca^{2+} transients
572 and their features (peak amplitude and width at half-maximum) were identified from ratio traces
573 using the *findpeaks* algorithm in MATLAB, and peaks were confirmed by visual inspection of
574 GCaMP5/mCherry recordings and ratio traces. Egg-laying events were observed by allowing a
575 small amount of bright field light to transmit into the mCherry channel whose gain was
576 increased for egg visualization. The egg-laying active state was defined in recordings to
577 include those transients that occurred one minute before and one minute after each egg-laying
578 event. Those transients not found within an active state were considered to be in the inactive
579 state. Inter-transient intervals were calculated by measuring the elapsed time between
580 successive Ca^{2+} transient peaks during the inactive and active state. Because some inactive
581 states were devoid of detectable activity (e.g. Figure 1F, VC Ca^{2+}), inter-transient intervals
582 during such periods were operationally defined as the time before the first or after the last
583 transient in the recording. Because the recordings were cropped to focus on the egg-laying
584 active state, the inactive state inter-transient intervals reported here should be considered a
585 lower estimate. To facilitate comparisons of ΔR/R between different reporters and recording
586 conditions (Figure 1H and 5D), the maximum peak amplitude was normalized to 1. Spectral
587 analysis of active phase Ca^{2+} traces was performed by Fast Fourier Transform method of
588 estimation using the Signal Analyzer app in the MATLAB Signal Processing toolbox (R2016b).
589 Quantitatively similar results were obtained using the Lomb-Scargle periodogram function and
590 using auto-correlation analysis (data not shown). The largest amplitude frequency peak
591 between 0 and 250 mHz from each active state periodogram was compared using one-way
592 ANOVA.

593

594 Locomotion phasing analysis

595 We recorded the position of the vulva during each sinusoidal body bend of locomotion relative
596 to observed HSN, VC, and vulval muscle Ca^{2+} transients. We recorded the timing of each
597 ventral contraction and/or relaxation flanking each Ca^{2+} transient peak. To approximate the
598 phasing of that Ca^{2+} relative to locomotion, we operationally defined 0° and 360° as when the
599 vulva was positioned when the adjacent body wall muscles were at their most ventrally
600 contracted state, and we defined 180° when the vulva was positioned when the adjacent body
601 wall muscles were at their most relaxed state. The relative timing of each Ca^{2+} transient peak
602 or behavior event was calculated as fraction of time elapsed between the previous and
603 subsequent contraction or relaxation, regardless of whether the animal was engaged in
604 forward or reverse locomotion, as described previously (Collins and Koelle, 2013). For
605 example, if a Ca^{2+} transient peaked exactly 2 seconds after the vulva passed through its most
606 ventrally relaxed state (180°) and 2 seconds prior to the ventral contracted state (360°), the
607 Ca^{2+} transient phasing would be halfway between 180° and 360°, or 270°. If a Ca^{2+} transient
608 peaked halfway between ventral contraction (0°) and ventral relaxation (180°), the Ca^{2+}
609 transient phasing of that peak would be 90°. This method of estimation allows for phasing
610 information to be extracted and compared independent of differences in individual animal
611 speed and locomotion direction.

612

613 Optogenetics

614 Channelrhodopsin-2 (ChR2) expressing strains were grown in the presence or absence of the
615 ChR2 cofactor all-*trans* retinal (ATR). ATR was prepared at 100mM in 100% ethanol and

616 stored at -20°C. To prepare NGM plates for behavior analysis, ATR was diluted to 0.4 mM with
617 warmed cultures of OP50 bacteria in B Broth, and 200 μl of culture was seeded onto each 60
618 mm NGM plate. The plates were allowed to grow for 24 hours at 25-37°C, after which late L4
619 worms were staged onto prepared plates for behavioral assays 24 hours later. During Ca^{2+}
620 imaging experiments, ChR2 was activated with the same light used for GCaMP5 excitation.
621 For timed behavior recording experiments on plates, a OTPG_4 TTL Pulse Generator (Doric
622 Optics) was used to trigger image capture (Grasshopper 3, 4.1 Megapixel, USB3 CMOS
623 camera, Point Grey Research) and shutter opening on a EL6000 metal halide light source
624 generating 8-16 mW/cm^2 (depending on the magnification used) of ~470±20nm blue light via a
625 EGFP filter set mounted on a Leica M165FC stereomicroscope. Worm size, speed, and body
626 bends were determined from image sequences using Volocity.

627

628 Tyramine behavior assays

629 Three adult animals were placed onto each of three 35 mm agar plates prepared with
630 tyramine-HCl (Sigma) and acetic acid seeded with OP50 bacteria as described (Pirri et al.,
631 2009). The average number of eggs laid was counted after 30 minutes from at least 11 trials
632 for each genotype and tyramine concentration.

633

634 Statistical analyses

635 Data were analyzed using Prism 6 (GraphPad). Average peak transient rhythm, worm speed,
636 worm length, body bends, or eggs laid were compared using one-way ANOVA with Bonferroni
637 correction for multiple comparisons, and error bars indicate 95% confidence intervals for the

638 mean. Ca^{2+} transient peak amplitudes, widths, and inter-transient intervals were pooled from
639 multiple animals (n≥4 animals per genotype/condition per experiment), compared using the
640 Mann-Whitney test (for pair-wise comparisons) or the Kruskal-Wallis test with Dunn's
641 correction (for multiple comparisons), and error bars indicate quartile intervals for the indicated
642 median. $p<0.05$ interactions were deemed significant and are labeled with an asterisk. *p* values
643 for specific interactions are indicated in the Figure legends. Sample sizes for behavioral assays
644 followed previous studies (Waggoner et al., 1998; Chase and Koelle, 2004; Collins and Koelle,
645 2013). The number of animals analyzed in each experiment is indicated below, with each Ca^{2+}
646 transient or egg-laying event serving as a biological replicate.

647 *Figures 1, 2, and Figure 2–figure supplement 1:* HSN, 235 inactive and 157 active state
648 intervals between 319 no-egg and 49 egg-laying transients from 11 animals; VC, 22 inactive
649 and 83 active state intervals between 59 no-egg and 32 egg-laying transients from 8 animals;
650 vulval muscles, 73 inactive and 136 active state intervals between 175 twitch (no-egg) and 37
651 egg-laying transients from 7 animals.

652 *Figure 3:* A, ±ATR, 7 animals; B, -ATR, 9 animals; +ATR, 10 animals; C, 52 egg-laying events
653 from 17 HSN-ChR2 +ATR animals; D-F (all genotypes), -ATR, 18 animals; +ATR, 17 animals.

654 *Figure 4:* A-E, wild type -FUDR, 150 inactive and 87 active state intervals between 221 twitch
655 (no-egg) and 17 egg-laying transients from 4 animals; wild-type +FUDR, 62 inactive state
656 intervals between 59 twitch (no-egg) transients from 4 animals; *egl-1(n986dm)* -FUDR, 450
657 inactive and 97 active state intervals between 531 twitch (no-egg) and 14 egg-laying transients
658 from 7 animals; *egl-1(n986dm)* +FUDR, 228 inactive state intervals between 222 twitch (no-
659 egg) transients from 6 animals.

660 *Figure 4–figure supplement 1:* A-C, 239 twitch (no-egg) transients and 22 egg-laying
661 transients from 5 untreated wild-type animals (A) and 91 twitch (no-egg) transients from 5
662 FUDR-treated wild-type animals (B); D-F, 550 twitch (no-egg) transients and 18 egg-laying
663 transients from 7 untreated *egl-1(n986dm)* animals (D) and 232 twitch (no-egg) transients from
664 8 FUDR-treated *egl-1(n986dm)* animals (E).

665 *Figure 5:* uv1, 24 inactive and 42 active state intervals for 16 no-egg and 51 egg-laying
666 transients from 13 animals.

667 *Figure 6:* A, wild-type, 60 animals analyzed per tyramine concentration, 3 animals on each of
668 20 plates containing either water or 15 mM tyramine; *lgc-55(tm2813)*, *tdc-1(n3419)*, *ser-*
669 *2(pk1357)*, and *tyra-3(ok325)* mutants, 45 animals analyzed per tyramine concentration, 3
670 animals on each of 15 plates containing either water or 15 mM tyramine. B, 30 animals
671 analyzed per tyramine concentration, 3 animals on each of 10 plates. C, 150 animals per
672 genotype and transgene, 3 animals on each of 10 plates with or without tyramine from 5
673 separate transgenic lines. D-E, wild-type, 235 inactive and 157 active state intervals from 11
674 animals; *lgc-55(tm2913)*, 368 inactive and 101 active state intervals from 9 animals.

675

Acknowledgments

This work was funded by a postdoctoral fellowship from the American Heart Association to KMC (POST4990016) and by grants from the NINDS to MRK (NS036918) and to MRK and KMC (NS086932). Confocal instrumentation was supported by a grant to the Yale Liver Center (DK34989). Some strains were provided by the *C. elegans* Genetics Center, which is funded by NIH Office of Research Infrastructure Programs (P40 OD010440). We thank members of the Koelle and Collins labs, and Drs. James Baker, Julia Dallman, Mike Francis, Mason Klein, and Sheyum Syed for comments and helpful discussions on the manuscript.

Competing Interests

The authors declare no financial and non-financial competing interests.

688 **References**

689 Akerboom J et al. (2012) Optimization of a GCaMP calcium indicator for neural activity imaging.
690 J Neurosci 32:13819–13840.

691 Alkema MJ, Hunter-Ensor M, Ringstad N, Horvitz HR (2005) Tyramine Functions
692 independently of octopamine in the *Caenorhabditis elegans* nervous system. Neuron
693 46:247–260.

694 Bany IA, Dong M-Q, Koelle MR (2003) Genetic and cellular basis for acetylcholine inhibition of
695 *Caenorhabditis elegans* egg-laying behavior. J Neurosci 23:8060–8069.

696 Bellemer A, Hirata T, Romero MF, Koelle MR (2011) Two types of chloride transporters are
697 required for GABA(A) receptor-mediated inhibition in *C. elegans*. EMBO J 30:1852–
698 1863.

699 Brenner S (1974) The genetics of *Caenorhabditis elegans*. Genetics 77:71–94.

700 Brundage L, Avery L, Katz A, Kim UJ, Mendel JE, Sternberg PW, Simon MI (1996) Mutations
701 in a *C. elegans* Gqalpha gene disrupt movement, egg laying, and viability. Neuron
702 16:999–1009.

703 Carnell L, Illi J, Hong SW, McIntire SL (2005) The G-protein-coupled serotonin receptor SER-1
704 regulates egg laying and male mating behaviors in *Caenorhabditis elegans*. J Neurosci
705 25:10671–10681.

706 Chase DL, Koelle MR (2004) Genetic analysis of RGS protein function in *Caenorhabditis*
707 *elegans*. Methods Enzymol 389:305–320.

708 Collins KM, Koelle MR (2013) Postsynaptic ERG Potassium Channels Limit Muscle Excitability
709 to Allow Distinct Egg-Laying Behavior States in *Caenorhabditis elegans*. J Neurosci Off
710 J Soc Neurosci 33:761–775.

711 Daniels SA, Ailion M, Thomas JH, Sengupta P (2000) egl-4 acts through a transforming growth
712 factor-beta/SMAD pathway in *Caenorhabditis elegans* to regulate multiple neuronal
713 circuits in response to sensory cues. Genetics 156:123–141.

714 Desai C, Garriga G, McIntire SL, Horvitz HR (1988) A genetic pathway for the development of
715 the *Caenorhabditis elegans* HSN motor neurons. Nature 336:638–646.

716 Dong MQ, Chase D, Patikoglou GA, Koelle MR (2000) Multiple RGS proteins alter neural G
717 protein signaling to allow *C. elegans* to rapidly change behavior when fed. Genes Dev
718 14:2003–2014.

719 Elkes DA, Cardozo DL, Madison J, Kaplan JM (1997) EGL-36 Shaw channels regulate *C.*
720 *elegans* egg-laying muscle activity. Neuron 19:165–174.

721 Emtage L, Aziz-Zaman S, Padovan-Merhar O, Horvitz HR, Fang-Yen C, Ringstad N (2012)
722 IRK-1 Potassium Channels Mediate Peptidergic Inhibition of *Caenorhabditis elegans*
723 Serotonin Neurons via a Go Signaling Pathway. J Neurosci 32:16285–16295.

724 Erbguth K, Prigge M, Schneider F, Hegemann P, Gottschalk A (2012) Bimodal activation of
725 different neuron classes with the spectrally red-shifted channelrhodopsin chimera C1V1
726 in *Caenorhabditis elegans*. PloS One 7:e46827.

727 Fujiwara M, Aoyama I, Hino T, Teramoto T, Ishihara T (2016) Gonadal Maturation Changes
728 Chemotaxis Behavior and Neural Processing in the Olfactory Circuit of *Caenorhabditis*
729 *elegans*. Curr Biol 26:1522–1531.

730 Hajdu-Cronin YM, Chen WJ, Patikoglou G, Koelle MR, Sternberg PW (1999) Antagonism
731 between G(o)alpha and G(q)alpha in *Caenorhabditis elegans*: the RGS protein EAT-16
732 is necessary for G(o)alpha signaling and regulates G(q)alpha activity. Genes Dev
733 13:1780–1793.

734 Hallem EA, Spencer WC, McWhirter RD, Zeller G, Henz SR, Rätsch G, Miller DM, Horvitz HR,
735 Sternberg PW, Ringstad N (2011) Receptor-type guanylate cyclase is required for
736 carbon dioxide sensation by *Caenorhabditis elegans*. Proc Natl Acad Sci U S A
737 108:254–259.

738 Hapiak VM, Hobson RJ, Hughes L, Smith K, Harris G, Condon C, Komuniecki P, Komuniecki
739 RW (2009) Dual excitatory and inhibitory serotonergic inputs modulate egg laying in
740 *Caenorhabditis elegans*. Genetics 181:153–163.

741 Hardaker LA, Singer E, Kerr R, Zhou G, Schafer WR (2001) Serotonin modulates locomotory
742 behavior and coordinates egg-laying and movement in *Caenorhabditis elegans*. J
743 Neurobiol 49:303–313.

744 Hobson RJ, Hapiak VM, Xiao H, Buehrer KL, Komuniecki PR, Komuniecki RW (2006) SER-7,
745 a *Caenorhabditis elegans* 5-HT7-like receptor, is essential for the 5-HT stimulation of
746 pharyngeal pumping and egg laying. Genetics 172:159–169.

747 Hu Z, Pym ECG, Babu K, Vashlishan Murray AB, Kaplan JM (2011) A neuropeptide-mediated
748 stretch response links muscle contraction to changes in neurotransmitter release.
749 Neuron 71:92–102.

750 Johnstone DB, Wei A, Butler A, Salkoff L, Thomas JH (1997) Behavioral defects in *C. elegans*
751 *egl-36* mutants result from potassium channels shifted in voltage-dependence of
752 activation. Neuron 19:151–164.

753 Jose AM, Bany IA, Chase DL, Koelle MR (2007) A specific subset of transient receptor
754 potential vanilloid-type channel subunits in *Caenorhabditis elegans* endocrine cells
755 function as mixed heteromers to promote neurotransmitter release. Genetics 175:93–
756 105.

757 Jospin M, Jacquemond V, Mariol M-C, Segalat L, Allard B (2002) The L-type voltage-
758 dependent Ca^{2+} channel EGL-19 controls body wall muscle function in *Caenorhabditis*
759 *elegans*. J Cell Biol 159:337–348.

760 Kariya K-I, Bui YK, Gao X, Sternberg PW, Kataoka T (2004) Phospholipase Cε regulates
761 ovulation in *Caenorhabditis elegans*. Dev Biol 274:201–210.

762 Kim J, Poole DS, Waggoner LE, Kempf A, Ramirez DS, Treschow PA, Schafer WR (2001)
763 Genes affecting the activity of nicotinic receptors involved in *Caenorhabditis elegans*
764 egg-laying behavior. Genetics 157:1599–1610.

765 Koelle MR, Horvitz HR (1996) EGL-10 regulates G protein signaling in the *C. elegans* nervous
766 system and shares a conserved domain with many mammalian proteins. Cell 84:115–
767 125.

768 Lee RY, Lobel L, Hengartner M, Horvitz HR, Avery L (1997) Mutations in the alpha1 subunit of
769 an L-type voltage-activated Ca^{2+} channel cause myotonia in *Caenorhabditis elegans*.
770 EMBO J 16:6066–6076.

771 Li P, Collins KM, Koelle MR, Shen K (2013) LIN-12/Notch signaling instructs postsynaptic
772 muscle arm development by regulating UNC-40/DCC and MADD-2 in *Caenorhabditis*
773 *elegans*. eLife 2:e00378.

774 Liu DW, Thomas JH (1994) Regulation of a periodic motor program in *C. elegans*. J Neurosci
775 14:1953–1962.

776 Marder E (2012) Neuromodulation of neuronal circuits: back to the future. Neuron 76:1–11.

777 Marder E, Goeritz ML, Otopalik AG (2015) Robust circuit rhythms in small circuits arise from
778 variable circuit components and mechanisms. Curr Opin Neurobiol 31:156–163.

779 McCarter J, Bartlett B, Dang T, Schedl T (1999) On the control of oocyte meiotic maturation
780 and ovulation in *Caenorhabditis elegans*. Dev Biol 205:111–128.

781 Miller KG, Emerson MD, Rand JB (1999) Goalpha and diacylglycerol kinase negatively
782 regulate the Gqalpha pathway in *C. elegans*. Neuron 24:323–333.

783 Mitchell DH, Stiles JW, Santelli J, Sanadi DR (1979) Synchronous growth and aging of
784 *Caenorhabditis elegans* in the presence of fluorodeoxyuridine. J Gerontol 34:28–36.

785 Moresco JJ, Koelle MR (2004) Activation of EGL-47, a Galpha(o)-coupled receptor, inhibits
786 function of hermaphrodite-specific motor neurons to regulate *Caenorhabditis elegans*
787 egg-laying behavior. J Neurosci 24:8522–8530.

788 Nagel G, Brauner M, Liewald JF, Adeishvili N, Bamberg E, Gottschalk A (2005) Light activation
789 of channelrhodopsin-2 in excitable cells of *Caenorhabditis elegans* triggers rapid
790 behavioral responses. Curr Biol 15:2279–2284.

791 Newman AP, Sternberg PW (1996) Coordinated morphogenesis of epithelia during
792 development of the *Caenorhabditis elegans* uterine-vulval connection. Proc Natl Acad
793 Sci 93:9329–9333.

794 Newman AP, White JG, Sternberg PW (1996) Morphogenesis of the *C. elegans* hermaphrodite
795 uterus. Dev Camb Engl 122:3617–3626.

796 Pirri JK, McPherson AD, Donnelly JL, Francis MM, Alkema MJ (2009) A tyramine-gated
797 chloride channel coordinates distinct motor programs of a *Caenorhabditis elegans*
798 escape response. Neuron 62:526–538.

799 Porter MY, Xie K, Pozharski E, Koelle MR, Martemyanov KA (2010) A Conserved Protein
800 Interaction Interface on the Type 5 G Protein β Subunit Controls Proteolytic Stability and
801 Activity of R7 Family Regulator of G Protein Signaling Proteins. J Biol Chem
802 285:41100–41112.

803 Ringstad N, Horvitz HR (2008) FMRFamide neuropeptides and acetylcholine synergistically
804 inhibit egg-laying by *C. elegans*. Nat Neurosci 11:1168–1176.

805 Sarov M et al. (2012) A genome-scale resource for in vivo tag-based protein function
806 exploration in *C. elegans*. Cell 150:855–866.

807 Schafer WF (2006) Genetics of egg-laying in worms. Annu Rev Genet 40:487–509.

808 Shyn SI, Kerr R, Schafer WR (2003) Serotonin and Go modulate functional states of neurons
809 and muscles controlling *C. elegans* egg-laying behavior. Curr Biol 13:1910–1915.

810 Tanis JE, Bellemer A, Moresco JJ, Forbush B, Koelle MR (2009) The potassium chloride
811 cotransporter KCC-2 coordinates development of inhibitory neurotransmission and
812 synapse structure in *Caenorhabditis elegans*. J Neurosci 29:9943–9954.

813 Tanis JE, Moresco JJ, Lindquist RA, Koelle MR (2008) Regulation of serotonin biosynthesis by
814 the G proteins Galphao and Galphaq controls serotonin signaling in Caenorhabditis
815 elegans. Genetics 178:157–169.

816 Topalidou I, Keller C, Kalebic N, Nguyen KCQ, Somhegyi H, Politi KA, Heppenstall P, Hall DH,
817 Chalfie M (2012) Genetically separable functions of the MEC-17 tubulin
818 acetyltransferase affect microtubule organization. Curr Biol 22:1057–1065.

819 Trent C, Tsuing N, Horvitz HR (1983) Egg-laying defective mutants of the nematode
820 *Caenorhabditis elegans*. Genetics 104:619–647.

821 Waggoner LE, Dickinson KA, Poole DS, Tabuse Y, Miwa J, Schafer WR (2000) Long-term
822 nicotine adaptation in *Caenorhabditis elegans* involves PKC-dependent changes in
823 nicotinic receptor abundance. J Neurosci 20:8802–8811.

824 Waggoner LE, Zhou GT, Schafer RW, Schafer WR (1998) Control of alternative behavioral
825 states by serotonin in *Caenorhabditis elegans*. Neuron 21:203–214.

826 Weinshenker D, Garriga G, Thomas JH (1995) Genetic and pharmacological analysis of
827 neurotransmitters controlling egg laying in *C. elegans*. J Neurosci 15:6975–6985.

828 Weinshenker D, Wei A, Salkoff L, Thomas JH (1999) Block of an ether-a-go-go-like K(+)
829 channel by imipramine rescues *egl-2* excitation defects in *Caenorhabditis elegans*. J
830 Neurosci 19:9831–9840.

831 White JG, Southgate E, Thomson JN, Brenner S (1976) The structure of the ventral nerve cord
832 of *Caenorhabditis elegans*. Philos Trans R Soc Lond B Biol Sci 275:327–348.

833 White, J.G., Southgate, E., Thomson, J.N., Brenner, S. (1986) The structure of the nervous
834 system of the nematode *Caenorhabditis elegans*. Phil Trans R Soc 314:1–340.

835 Williams SL, Lutz S, Charlie NK, Vettel C, Ailion M, Coco C, Tesmer JJG, Jorgensen EM,
836 Wieland T, Miller KG (2007) Trio's Rho-specific GEF domain is the missing Galpha q
837 effector in *C. elegans*. Genes Dev 21:2731–2746.

838 Zhang M, Chung SH, Fang-Yen C, Craig C, Kerr RA, Suzuki H, Samuel ADT, Mazur E,
839 Schafer WR (2008) A self-regulating feed-forward circuit controlling *C. elegans* egg-
840 laying behavior. Curr Biol 18:1445–1455.

841 Zhang M, Schafer WR, Breitling R (2010) A circuit model of the temporal pattern generator of
842 *Caenorhabditis* egg-laying behavior. BMC Syst Biol 4:81.

843

844 **Figure 1.** Cell-specific reporters of activity in the *C. elegans* egg-laying behavior circuit.

845 (**A**) Schematic of the circuit. HSN (green) and VC (blue) motor neurons synapse onto the vm2
846 muscle postsynaptic termini (center of schematic). The uv1 neuroendocrine cells (pink) extend
847 processes (grey) along the vulval slit and vm2 postsynaptic terminus. (**B-E**) Individual video
848 frames of the GCaMP5:mCherry fluorescence ratio showing active state Ca^{2+} transients in
849 HSNs (**B**), VCs (**C**), and vulval muscles during twitching (**D**) and egg-laying behaviors (**E**).
850 Arrowheads, HSN and VC presynaptic termini; asterisks, cell bodies; scale bar, 10 μm. (**F**) 30
851 minute recordings of HSN, VC, and vulval muscle activity (left panel), showing distinct active
852 (yellow) and inactive (grey) egg-laying behavior states, with expanded timescale of one active
853 state at right. Arrowheads show egg-laying events. (**G**) Scatter plots and median HSN, VC, and
854 vulval muscle (vm) inter-transient intervals during egg-laying inactive (–, filled circles) and
855 active (+, open circles) states. Asterisks indicate significant differences (p<0.0001). (**H**)
856 Relationship between Ca^{2+} transient amplitude and egg release. Scatter plots and medians of
857 normalized amplitude with (+; open circles) and without (–; closed circles) egg release. Also
858 shown is the percent of total transients that accompanied egg release. (**I**) Timing of HSN, VC,
859 and vulval muscle Ca^{2+} transients and egg release. Shown at top is a curve of the median of
860 Ca^{2+} from HSN (green), VC (blue), and vulval muscles (orange) from normalized $\Delta R/R$ traces
861 (with the peak Ca^{2+} set to 100%) synchronized to the moment of egg release (0 s, arrowhead
862 and dotted line). Bars indicate 20% change in median GCaMP5/mCherry ratio. The timing of
863 the HSN Ca^{2+} peak is significantly different from that of the VCs and vulval muscles (p<0.0001).
864 Shown at bottom is a trace of median vulval muscle size. Bar shows a 5% change in median
865 object size based on mCherry fluorescence.

866

867

868 **Figure 2.** HSN, VC, and vulval muscle activity is rhythmic and phased with animal locomotion.

869 (**A**) Active-state segments, such as the one shown here, were extracted from Ca^{2+} recordings,
870 and analyzed for rhythmicity by power spectrum analysis. Underlying rhythm frequencies and
871 peak inter-transient intervals were thus extracted for HSN (**B**), VC (**C**), and vulval muscle (**D**)
872 traces, and the peak of maximum rhythm for each active state is indicated in bold. (**E**) The
873 average vulval muscle Ca^{2+} peak interval (~10 s) was significantly different than the ~20 s
874 rhythm observed in HSN (p<0.0003) and VC (p<0.0006) Ca^{2+} recordings. HSN and VC
875 rhythms were not significantly different from each other (p>0.9999; one-way ANOVA). (**F**) The
876 position of the vulva within a sinusoidal locomotor body bend at the moment a Ca^{2+} transient
877 peaked was used to assign a body bend "phase", in units of degrees, with 180° representing
878 ventral relaxation and 0/360° representing ventral contraction. Plots show the percent of Ca^{2+}
879 transients observed in each of eight 45° bins for HSN (**G**), VC (**H**), and vulval muscle (**I**), with
880 data for transients accompanied by an egg-laying event ("egg transient") plotted in different
881 colors from data for transients not accompanied by an egg-laying event ("no egg transient").
882 These plots show data pooled from recordings of 8-11 animals, and Figure 2–figure
883 supplement 1 shows plots for each animal separately. The phasing of VC and vulval muscle
884 transients that did not lead to egg laying is significantly different from an equal number of
885 randomly distributed events (R, at 12.5%; p<0.0001; Kruskal-Wallis test).

886

887 **Figure 2–figure supplement 1.** Relative timing of HSN, VC, and vulval muscle Ca^{2+} transients
888 during locomotion body bends.

889 The position of the vulva within a sinusoidal locomotor body bend was used to assign a body
890 bend "phase", in units of degrees, for each Ca^{2+} transient analyzed in Figure 1 as described in
891 the Materials and Methods. The timing of each HSN (**A**), VC (**B**), or vulval muscle (**C**) Ca^{2+}
892 transient peak with egg release (open circles) or without egg release (closed circles) was
893 determined relative to the position of the vulva during the body bends of locomotion. Bar and
894 whisker plots indicate the median and quartiles for each transient phase.

895

896 **Figure 3.** Optogenetic activation of HSN neurons initiates the egg-laying active state, and
897 optogenetic activation of VC neurons slows locomotion.

898 **(A**) Animals expressing Channelrhodopsin-2 (ChR2) in the HSNs and GCaMP5/mCherry in the
899 VC neurons were grown in the presence (+ATR; top, blue) or absence (–ATR; bottom, black)
900 of all-*trans* retinal. 489 nm laser light was used to simultaneously stimulate ChR2 activity and
901 excite GCaMP5 fluorescence during the entire recording. Arrowheads indicate egg-laying
902 events. (**B**) The same experiment as (A) except that GCaMP5/mCherry were expressed in the
903 vulval muscles rather than VCs. (**C**) Brief reduction of animal speed during optogenetically-
904 induced egg laying. The egg-laying active state in animals expressing ChR2 in the HSN
905 neurons was induced with 30 s exposure to blue light. Average speed (black trace) about each
906 egg-laying event (0 s) was calculated from the worm centroid position, and the grey area
907 shows the 95% confidence interval. Average speed at the moment of egg laying release (0 s)
908 is reduced compared to 1 s before or after (p<0.001). See also Movie 4. (**D**) Activation of the
909 VC neurons slows locomotion but fails to induce egg laying. Animals expressing ChR2 in the
910 VCs were grown in the presence (+ATR; red) or absence (–ATR; black/grey) of all-*trans* retinal,
911 and worm length (upper photos and graph) was determined. Micrographs are still images from

912 a representative animal at indicated time points (see Movie 5). Inset arrows indicate regions of
913 the head and tail that remain mobile after VC activation. Scatter plots of body bends (**E**) and
914 egg laying (**F**) from the same recordings shown in D. There was a significant change in worm
915 length and body bends, but not egg laying, during blue light in animals grown on ATR (red;
916 $p<0.0001$). Positive control animals expressing ChR2 in the HSNs (green) showed a significant
917 increase in egg laying during blue light ($p<0.0001$).

918

919 **Figure 4.** Active states require egg production but not the HSNs.

920 (**A**) Vulval muscle activity in wild-type animals either untreated or after sterilization with
921 floxuridine (FUDR). Left panel shows 30-minute recordings with the grey underlined regions
922 expanded at right. (**B**) Vulval muscle activity in *egl-1(n986dm)* mutants lacking HSNs. (**C-D**)
923 Scatter plots of vulval muscle inter-transient intervals (**C**) and amplitudes (**D**). Line indicates
924 median, error bars indicate quartiles, and asterisks indicate significant differences ($p<0.01$). (**E**)
925 Vulval muscle transients are wider in animals lacking HSNs. Cumulative distribution plots of
926 Ca^{2+} transient peak widths; asterisk indicates $p<0.0001$ (Mann-Whitney test).

927

928 **Figure 4–figure supplement 1.** Persistent phasing of rhythmic vulval muscle activity in
929 animals lacking HSNs and after sterilization.

930 Phasing of vulval muscle Ca^{2+} transients during twitching (closed circles) and egg laying (open
931 circles) in five untreated wild-type animals (**A**) and five animals sterilized with FUDR (**B**). Bar
932 and whisker plots indicate the median and quartiles for each transient phase. (**C**) Histograms
933 of pooled data showing phasing of vulval muscle twitches (red) and egg-laying transients

934 (yellow) in untreated wild-type animals and twitches after FUDR treatment (blue). Phasing of
935 vulval muscle Ca^{2+} transients during twitching (closed circles) and egg laying (open circles) in
936 seven untreated *egl-1(n986dm)* mutant animals lacking HSNs (**D**) and eight *egl-1(n986dm)*
937 animals sterilized with FUDR (**E**). Bar and whisker plots indicate the median and quartiles for
938 each transient phase. (**F**) Histogram of pooled data showing phasing of vulval muscle twitches
939 (red) and egg-laying transients (yellow) in untreated *egl-1(n986dm)* animals and twitches after
940 FUDR treatment (blue).

941

942 **Figure 5.** The tyraminergic uv1 neuroendocrine cells are mechanically deformed and activated
943 by egg laying.

944 (**A**) Fluorescence micrographs of uv1 showing GCaMP5, mCherry, and the GCaMP5/mCherry
945 ratio before egg laying, during egg passage through the vulva, and after egg release. Times of
946 movie frames in seconds are at top, and white scale bar is 10 μm. Arrowheads in mCherry
947 micrographs indicate position of uv1 cells as they are deformed by egg passage, the dotted
948 line indicates position and opening of the vulva. (**B**) GCaMP5/mCherry ratio ($\Delta R/R$) trace of
949 uv1 activity, including an egg-laying active state. Egg-laying events are indicated by
950 arrowheads. (**C**) Scatter plots of uv1 inter-transient intervals during the inactive (closed circles)
951 and active (open circles) egg-laying behavior states. Line indicates median, error bars indicate
952 quartiles, and asterisks indicate significant differences ($p<0.0001$). (**D**) Scatter plots and
953 medians of normalized amplitude with (+; open circles) and without (–; closed circles) an
954 accompanying egg release. Error bars indicate quartiles, and asterisks indicate significant
955 differences ($p<0.0001$, Mann-Whitney test). (**E**) uv1 Ca^{2+} transients follow egg-laying events.
956 Normalized traces of median Ca^{2+} in HSN (green) and VC (blue) from Figure 1 are compared

957 to uv1 (purple), synchronized to the moment of egg release (0 s, arrowhead and dotted line).
958 Bars indicate 20% change in median GCaMP5/mCherry ratio. Asterisk indicates the uv1 Ca^{2+}
959 peak is significantly later than the HSN and VC peaks (p<0.0001).

960

961 **Figure 6.** Tyramine inhibits egg laying, in part, through LGC-55 receptors on the HSNs.

962 (**A**) Exogenous tyramine inhibits egg-laying behavior and requires the LGC-55 receptor.
963 Scatter plots and means showing the average number of eggs laid after 30 minutes by wild
964 type (grey), *tdc-1(n3419*) tyramine biosynthetic enzyme mutant (blue), and *lgc-55(tm2913),*
965 *ser-2(pk1357)*, and *tyra-3(ok325)* tyramine receptor mutant animals (orange, red, and purple,
966 respectively) on plates without (–, closed circles) or with (+, open circles) 15 mM tyramine.
967 Error bars indicate 95% confidence intervals, and asterisks indicate significant responses
968 (p<0.01) while n.s. is not significant (p>0.05). (**B**) Dose-response curve of tyramine inhibition
969 on egg laying in wild-type and *lgc-55* mutant animals. Asterisks indicate significant differences
970 at 10 mM (p<0.0001) and 20 mM tyramine (p=0.0164). (**C**) LGC-55 is expressed in HSN, uv1,
971 and vulval muscles. Expression of LGC-55 tagged with GFP compared to vulval muscle
972 mCherry was visualized using confocal microscopy; scale bar is 10 μm. GFP is localized to the
973 HSN and uv1 cell bodies (arrows) as well as the ventral tips of the vulval muscles. (**D**) Re-
974 expression of LGC-55 in HSN restores tyramine inhibition of egg laying. Scatter plots of eggs
975 laid by *lgc-55* mutants expressing either GFP or *lgc-55* in the HSN from the *tph-1* promoter.
976 Asterisk indicates significant differences in egg laying (p=0.0029). (**E**) Loss of LGC-55
977 increases HSN activity. Representative Ca^{2+} ratio traces show HSN activity in wild type (top,
978 grey) and *lgc-55* mutant animals (bottom, blue) during the active state. (**F**) Scatter plots and
979 medians of HSN inter-transient intervals in wild type and *lgc-55* mutant animals during the egg-

980 laying inactive (–, closed circles) and active (+, open circles) states. Asterisks indicate
981 statistically significant differences (p<0.0001).

982

983 **Figure 7.** Working model of how circuit connectivity, signaling, and activity contribute to the
984 observed rhythms that accompany the active and inactive egg-laying behavior states.

985 VA and VB motor neuron synapses release acetylcholine (ACh) that rhythmically excites the
986 body wall muscles (bwm) and vm1 vulval muscles during each locomotion body bend, every
987 ~10 seconds. Eggs are produced from each gonad arm every 10 minutes, and we propose the
988 accumulation of 2-3 eggs mechanically excites the uterine muscles (um) facilitating exit from
989 the inactive state. Sustained bursts of HSN command motor neuron activity trigger serotonin
990 release that drives ~2 minute active states. HSN also makes synapses and gap junctions with
991 the cholinergic VC motor neurons, and VC makes synapses and gap junctions with the vm2
992 muscles whose contraction allows egg release. Passage of eggs mechanically activates the
993 uv1 cells triggering release of tyramine and neuropeptides, which inhibit HSN activity to
994 terminate the active state. See text for further details.

995

996 **Movie 1.** Ratio recording of HSN Ca^{2+} transients during the egg-laying active state. High Ca^{2+}
997 is indicated in red while low calcium is in blue. Large panel is an expanded view showing the
998 freely-moving animal that has been contrast enhanced to make the worm and its laid eggs
999 visible. Inset is cropped to a small area containing the HSN, and stabilized to remove
1000 movement. Text labels indicate when Ca^{2+} transients and egg release occur.

1001 **Movie 2.** Ratio recording of VC Ca^{2+} transients during the egg-laying active state. High Ca^{2+}
1002 is indicated in red while low calcium is in blue. Contrast is enhanced to make the worm visible,
1003 although the laid eggs are not easily visible. Text labels indicate when vulval muscle (vm)
1004 twitches or egg-laying contractions occur, which result in small or large displacements of the
1005 VC4 and VC5 cell bodies, respectively.

1006 **Movie 3.** Ratio recording of vulval muscle Ca^{2+} transients during the egg-laying active state.
1007 High Ca^{2+} is indicated in red while low calcium is in blue. Large panel is an expanded view
1008 showing the freely-moving animal that has been contrast enhanced to make the worm and its
1009 laid eggs visible. Inset is cropped to a small area containing the vulval muscles, and stabilized
1010 to remove movement. Text labels indicate when Ca^{2+} transients and egg release occur.

1011 **Movie 4.** Activation of the HSNs using Channelrhodopsin-2 induces the egg-laying active state.
1012 Animals were recorded for a total of 90 seconds with continuous blue light stimulation
1013 beginning at 30 s and ending at 60s, during which five eggs are laid. Recording is sped up 3-
1014 fold.

1015 **Movie 5.** Activation of the VCs using Channelrhodopsin-2 induces animal paralysis and
1016 shortening of body length. Animals were recorded for a total of 90 seconds with continuous
1017 blue light stimulation beginning at 30 s and ending at 60s. Recording is sped up 3-fold.

1018 **Movie 6.** Ratio recording of uv1 Ca^{2+} transients during the egg-laying active state. High Ca^{2+}
1019 is indicated in red while low calcium is in blue. Large panel is an expanded view showing the
1020 freely-moving animal. Inset is cropped to a small area containing the uv1s, and stabilized to
1021 remove movement. Microscope is focused to image the two uv1 cells on the right side of this
1022 animal, while the two additional uv1 cells on the left side are out of focus and not visible. Text
1023 labels indicate when egg releases occur, each of which is followed by a uv1 Ca^{2+} transient.

1024

1025 **Table 1:** Strains used in this study

Strain	Feature	Genotype	Figures
LX1832	Strain for transgene production	*lite-1(ce314) lin-15(n765ts)* X	1-6
LX1836	HSN Channelrhodopsin	*wzIs30* IV; *lite-1(ce314) lin-15(n765ts)* X	3
LX1918	vulval muscle GCaMP5, mCherry	*lite-1(ce314) vsIs164 lin-15(n765ts)* X	1, 2, 3
LX1932	HSN Channelrhodopsin, vulval muscle GCaMP5, mCherry	*wzIs30* IV; *lite-1(ce314) vsIs164 lin-15(n765ts)* X	3
LX1938	No HSNs, vulval muscle GCaMP5, mCherry	*egl-1(n986dm)* V; *lite-1(ce314) vsIs164 lin-15(n765ts)* X	4
LX1986	uv1 GCaMP5, mCherry	*vsIs177*; *lite-1(ce314) lin-15(n765ts)* X	5
LX1960	VC GCaMP5, mCherry	*vsIs172*; *lite-1(ce314) lin-15(n765ts)* X	1, 2
LX1970	HSN Channelrhodopsin, VC GCaMP5, mCherry	*wzIs30* IV; *vsIs172*; *lite-1(ce314) lin-15(n765ts)* X	3
LX2004	HSN GCaMP5, mCherry	*lite-1(ce314), vsIs183 lin-15(n765ts)* X	1, 2, 6
LX2038	*lgc-55* null mutant HSN GCaMP5, mCherry	*lgc-55(tm2913)* V *lite-1(ce314) vsIs183 lin-15(n765ts)* X	6
MIA3	VC Channelrhodopsin	*keyIs3*; *lite-1(ce314) lin-15(n765ts)* X	3
MT13113	*tdc-1* null mutant; no tyramine biosynthesis	*tdc-1(n3419)* II	6
N2	Bristol strain	wild type	6
OH313	*ser-2* null mutant	*ser-2(pk1357)* X	6
VC125	*tyra-3* null mutant	*tyra-3(ok325)* X	6
QW89	*lgc-55* null mutant	*lgc-55(tm2913)* V	6
LX2096	vulval muscle mCherry	*vsIs191*; *lin-15(n765ts)* X	
LX2081	pan-neuronal TagRFP	*unc-119(ed3)* I; *otIs356*	
LX2137	vulval muscle mCherry, *lgc-55::gfp*	*vsIs191*; *vsEx791*	6
LX1330	*lgc-55* mutant expressing GFP in HSN from *tph-1* promoter	*lgc-55(tm2913)* V; *lin-15(n765ts)* X *vsEx557*	6
LX1329	*lgc-55* mutant expressing LGC-55 in HSN from *tph-1* promoter	*lgc-55(thm2913)* V; *lin-15(n765ts)* X *vsEx558*	6

1026

Collins et al., Figure 1

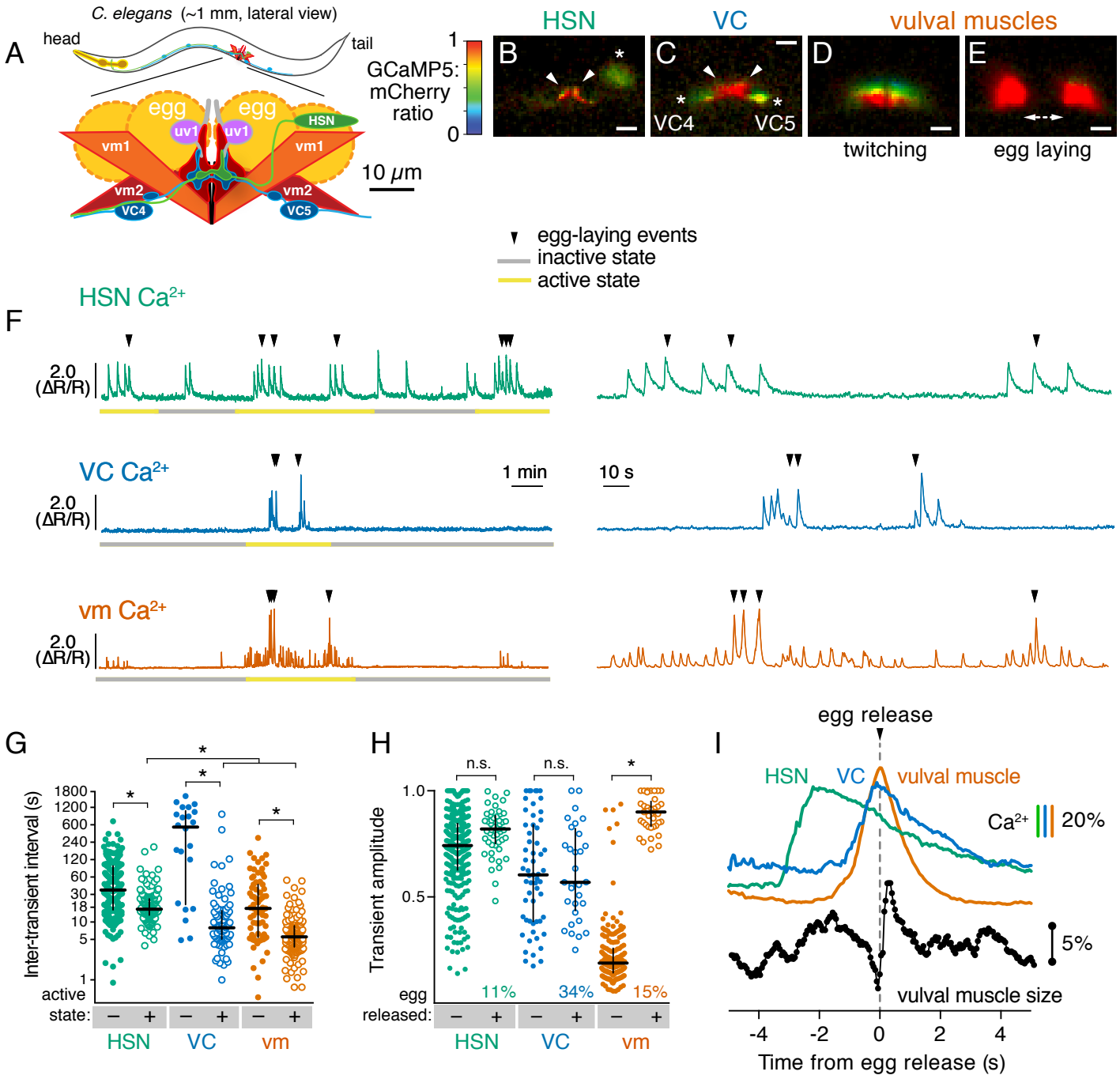

Collins et al., Figure 2

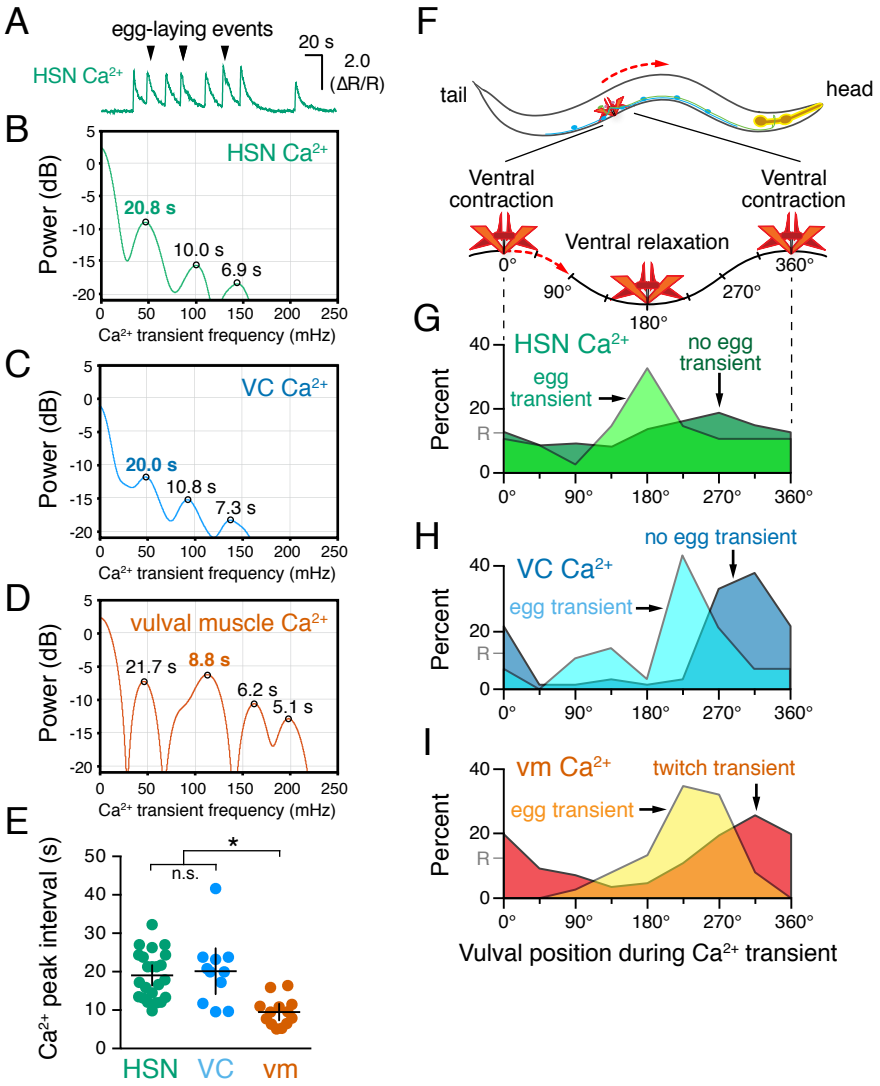

Collins et al., Figure 2 figure supplement 1

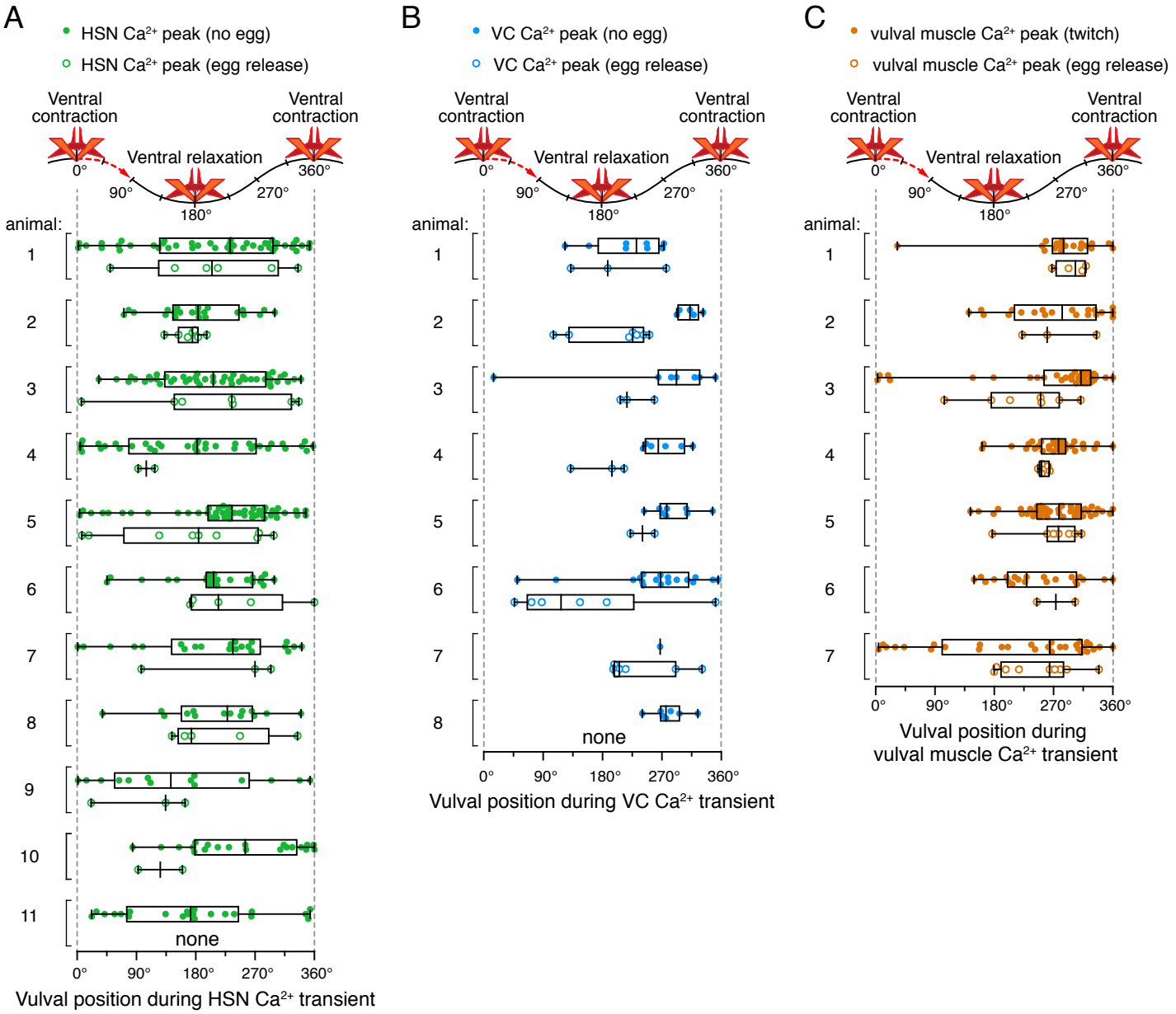

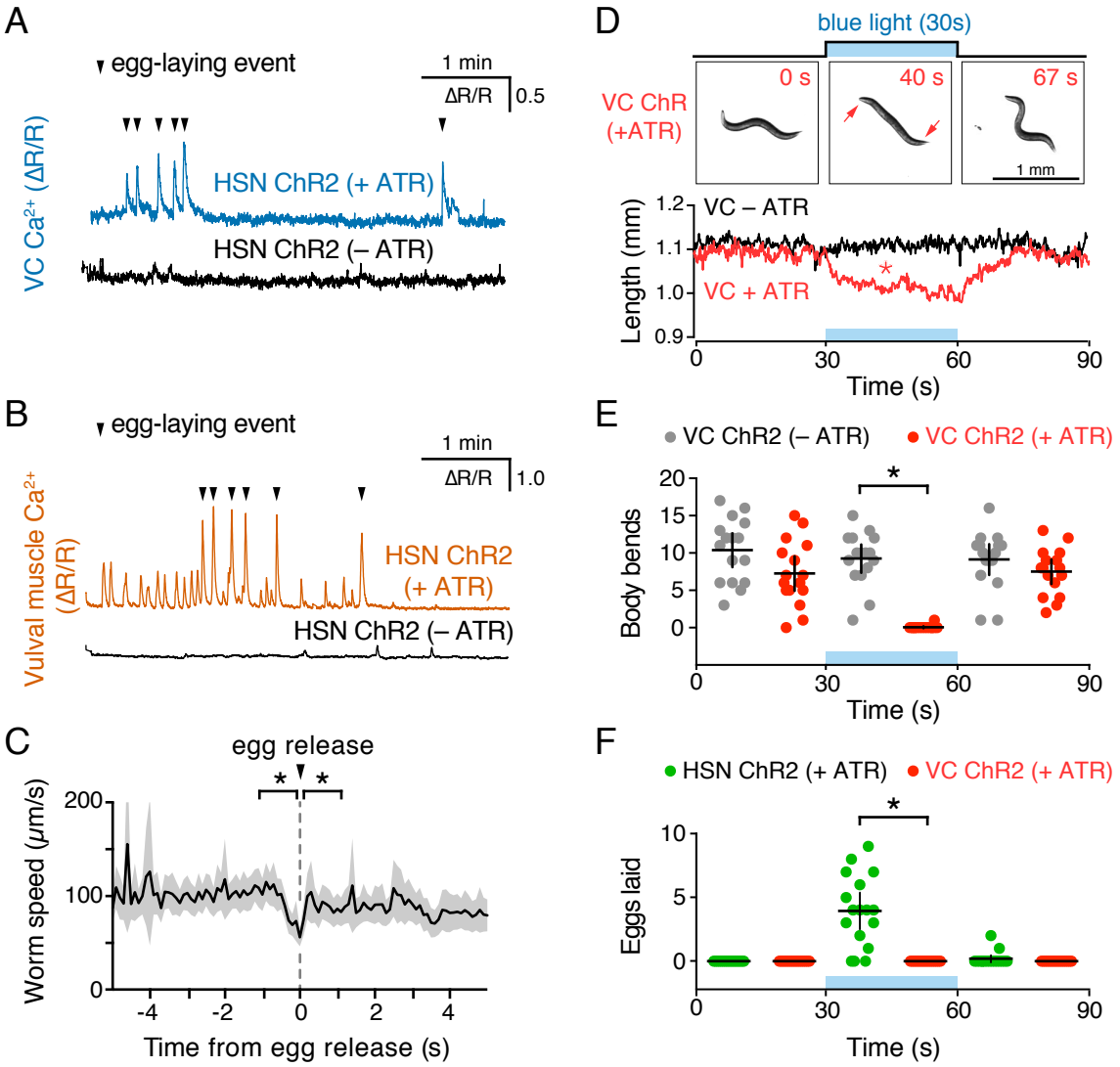
A
egg-laying event
1 min
ΔR/R
0.5
VC Ca2+ (ΔR/R)
HSN ChR2 (+ ATR)
HSN ChR2 (– ATR)
B
egg-laying event
1 min
ΔR/R
1.0
Vulval muscle Ca2+ (ΔR/R)
HSN ChR2 (+ ATR)
HSN ChR2 (– ATR)
C
egg release
Worm speed (μm/s)
200
100
0
-4
-2
0
2
4
Time from egg release (s)
D
blue light (30s)
VC ChR (+ATR)
0 s
40 s
67 s
1 mm
Length (mm)
1.2
1.1
1.0
0.9
VC – ATR
VC + ATR
0
30
60
90
Time (s)
E
VC ChR2 (– ATR)
VC ChR2 (+ ATR)
Body bends
20
15
10
5
0
Time (s)
F
HSN ChR2 (+ ATR)
VC ChR2 (+ ATR)
Eggs laid
10
5
0
Time (s)

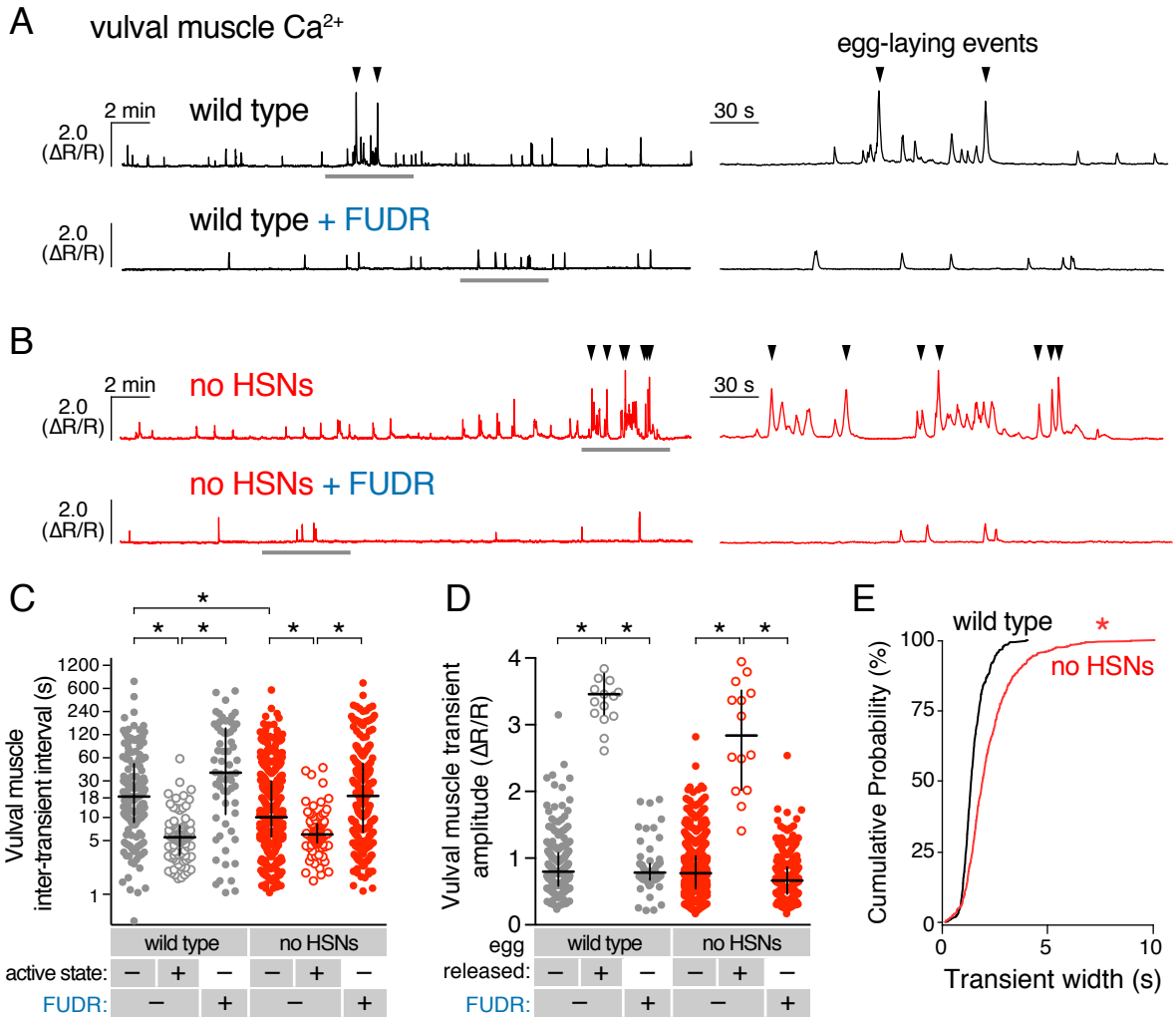
A
vulval muscle Ca2+
egg-laying events
2 min
wild type
30 s
2.0 (ΔR/R)
wild type + FUDR
B
no HSNs
no HSNs + FUDR
C
Vulval muscle inter-transient interval (s)
1200
600
240
120
60
30
18
10
5
1
wild type
no HSNs
active state:
FUDR:
D
Vulval muscle transient amplitude (ΔR/R)
egg released:
E
Cumulative Probability (%)
100
75
50
25
0
Transient width (s)
5
10

Collins et al., Figure 4 figure supplement 1

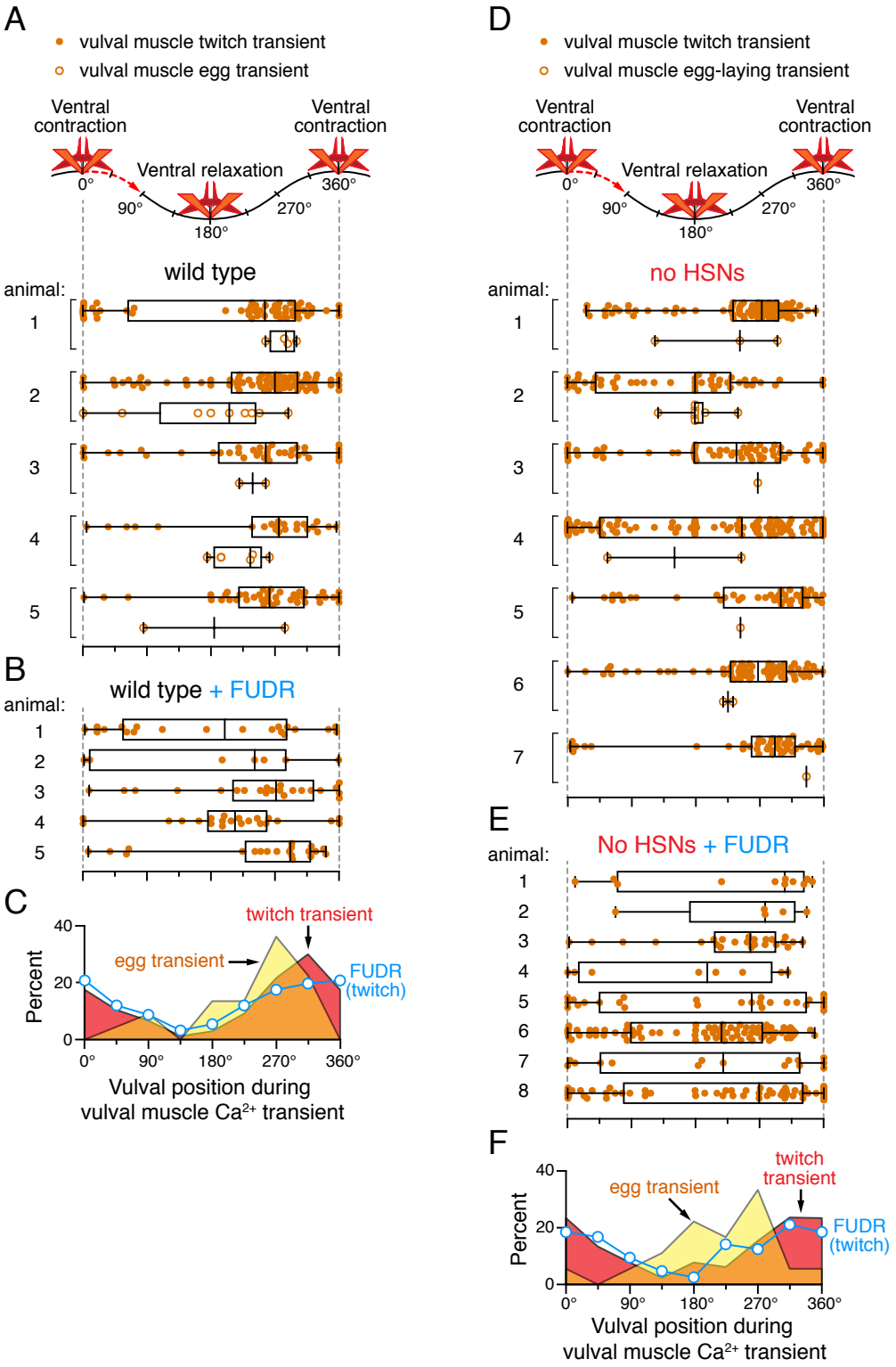

Collins et al., Figure 5

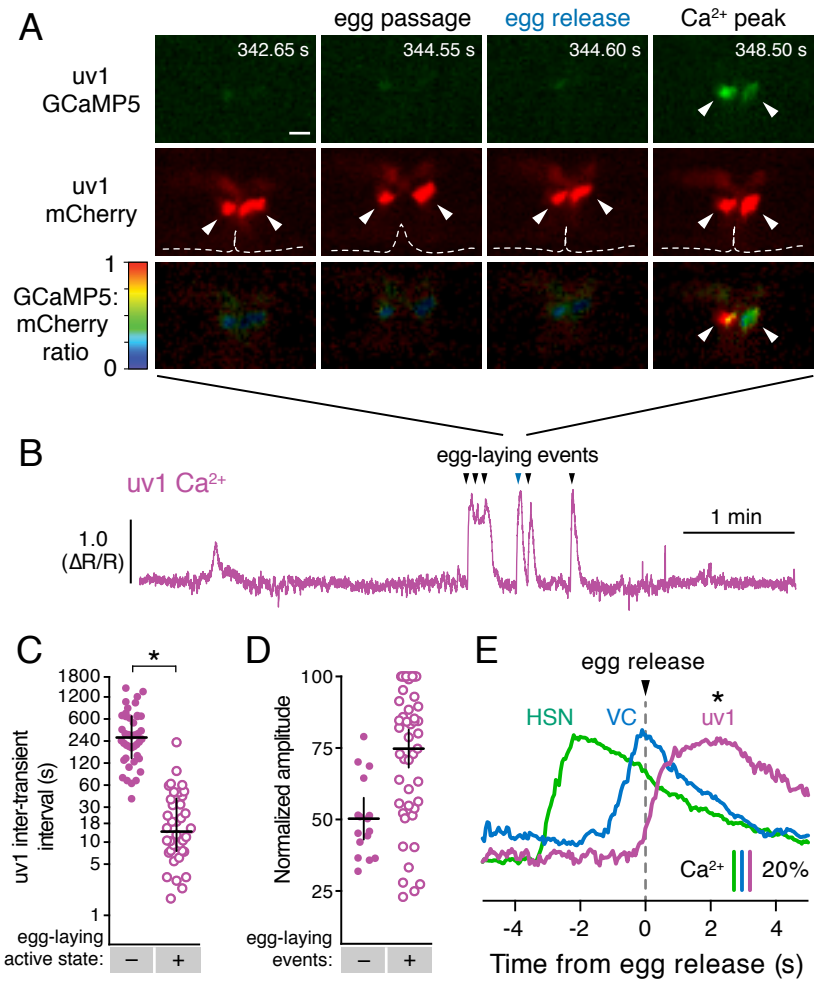

Collins et al., Figure 6

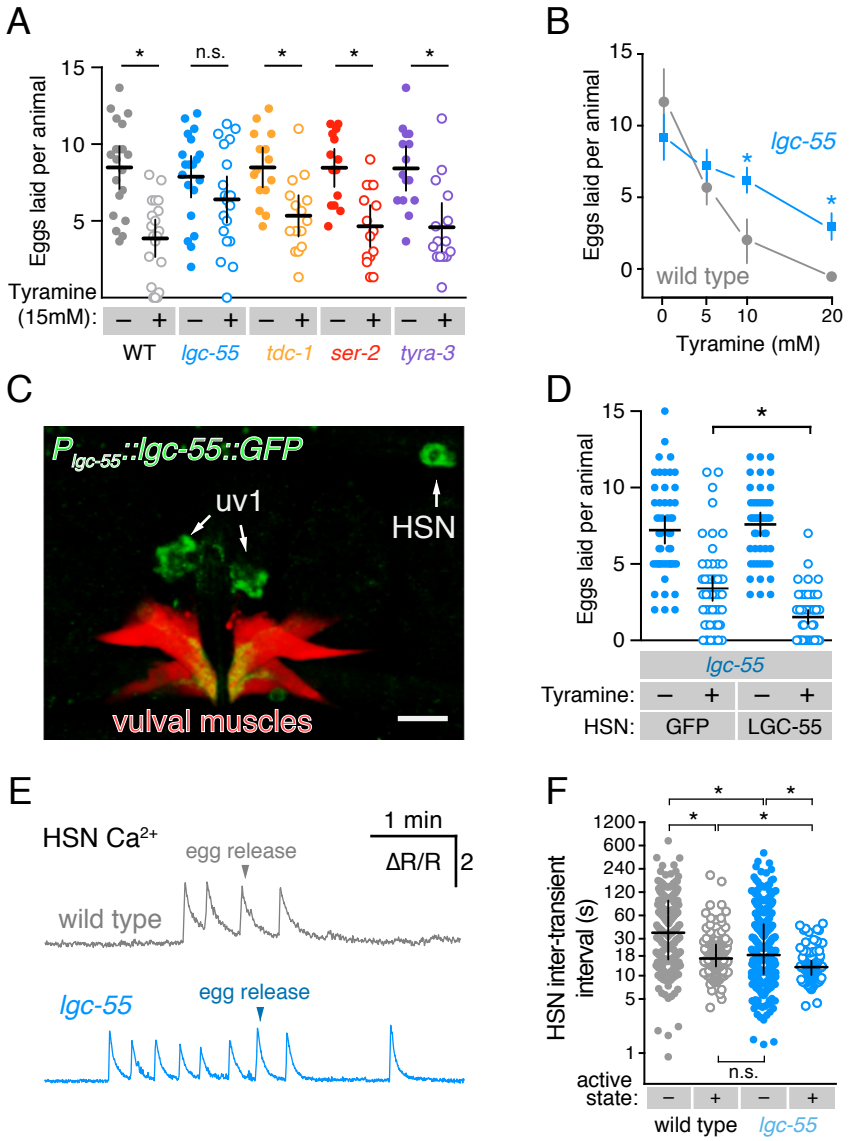
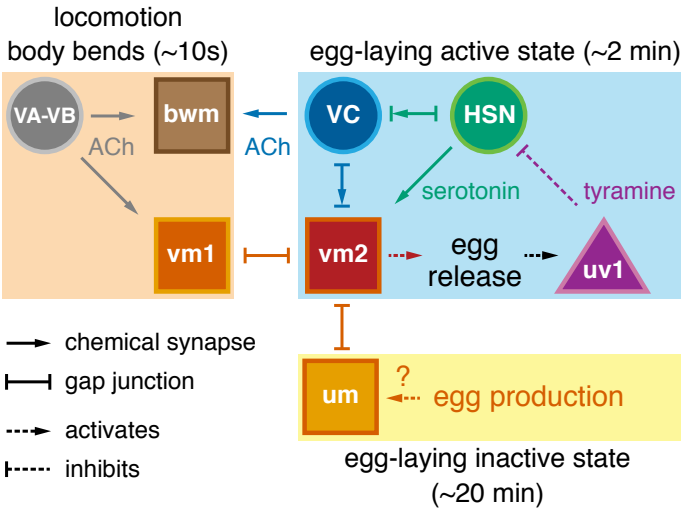
Collins et al., Figure 7